Tunable reducibility of alkaline earth metal clusters for carbon dioxide and nitrogen molecules activation: a QM-QSPR study

Natalia Wiszowska[1], Natalia Rogoża[1], Celina Sikorska[1,2,] [1]

[1] Faculty of Chemistry, University of Gdańsk,
Fahrenheit Union of Universities in Gdańsk, 80-308 Gdańsk, Poland

[2] Department of Physics, The University of Auckland
38 Princes Street, Auckland 1010, New Zealand

Supplementary Material

[1] Corresponding author: celina.sikorska@ug.edu.pl

1. Optimized structures of $BAe_3^{0/+/-}$ (Ae=Be, Mg, Ca) species

	neutral	cation	anion
BBe_2Mg	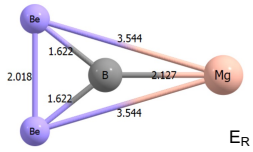 E_R = 0.56 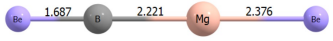 E_R = 2.98	No stable higher energy isomers were found	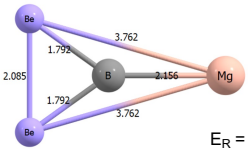 E_R = 0.48
$BBeMg_2$	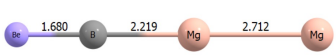 E_R = 2.62  E_R = 3.15 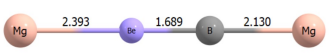 E_R = 1.79	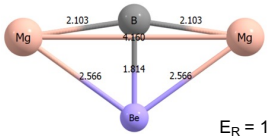 E_R = 1.12	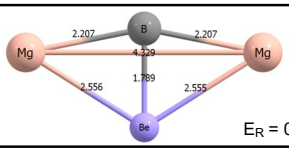 E_R = 0.16  E_R = 3.97  E_R = 4.06
BBe_2Ca	 E_R = 5.79	No stable higher energy isomers were found	No stable higher energy isomers were found
BMg_3	 E_R = 3.16	 E_R = 2.74	No stable higher energy isomers were found
$BBeCaMg$	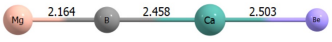 E_R = 4.72	No stable higher energy isomers were found	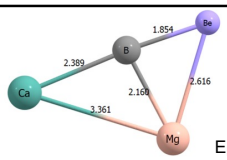 E_R = 0.68 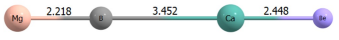 E_R = 4.37 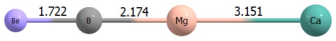 E_R = 3.64
$BCaMg_2$	No stable higher energy isomers were found	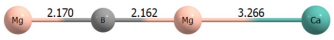 E_R = 2.73	No stable higher energy isomers were found
$BBeCa_2$	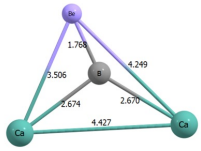 E_R = 0.34 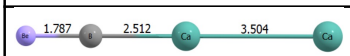 E_R = 2.50  E_R = 4.44	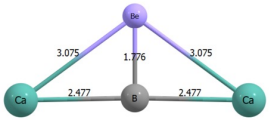 E_R = 0.17	No stable higher energy isomers were found
BCa_2Mg	No stable higher energy isomers were found	No stable higher energy isomers were found	 E_R = 2.95

Figure S 1 The MP2/6-311+G(d) equilibrium structures of $BAe_3^{0/+/-}$ (Ae=Be, Mg, Ca) species. Bond lengths in Å. The MP2/6-311+G(d) relative energies (E_r, in eV) are obtained for $BAe_3^{0/+/-}$ species with respect to the corresponding global minima (presented in Figure 1 of the main text).

2. Theory levels comparison

We performed geometry optimization for global minima at MP2/6-311+G(d) and MP2/6-311+G(3df) theory levels followed by energy calculation at the CCSD(T)/6-311+G(3df) level. The estimated ionization energy and electron affinity values are provided in Table S 1.

Table S 1 The lowest vibrational frequencies (V_1, in cm^{-1}), symmetry point group, adiabatic ionization energy (AIE, in eV), and adiabatic electron affinity (AEA, in eV) for the BAe_3 (Ae=Be, Mg, Ca) ground states.

Cluster	**Symmetry point group**	**V_1 (cm^{-1})** MP2/6-311+G(3df)	**CCSD(T)/6-311+(3df)//MP2/6-311+(3df)**		**V_1 (cm^{-1})** MP2/6-311+G(d)	**CCSD(T)/6-311+(3df)//MP2/6-311+(d)**	
			AIE (eV)	**AEA (eV)**		**AIE (eV)**	**AEA (eV)**
BBe_3	C_{3V}	450	6.827	1.993	535	6.758	2.067
BBe_2Mg	C_S	290	6.143	1.720	233	5.887	1.981
BMg_2Be	C_S	179	5.623	1.500	145	5.506	1.627
$BCaBe_2$	C_S	274	5.567	1.443	303	5.483	1.535
BMg_3	C_{3V}	158	5.216	1.312	153	5.221	1.321
BMgBeCa	C_1	147	5.189	1.309	123	5.137	1.371
$BCaMg_2$	C_S	136	4.896	1.184	85	4.762	1.339
BCa_2Be	C_S	118	4.830	1.175	78	4.433	1.578
BCa_2Mg	C_S	111	4.639	1.088	23	4.237	1.494
BCa_3	C_{3V}	122	4.460	0.995	38	3.729	1.706

3. Optimized structures of $BSr_3^{0/+/-}$ and $BSr_3^{0/+/-}$ species

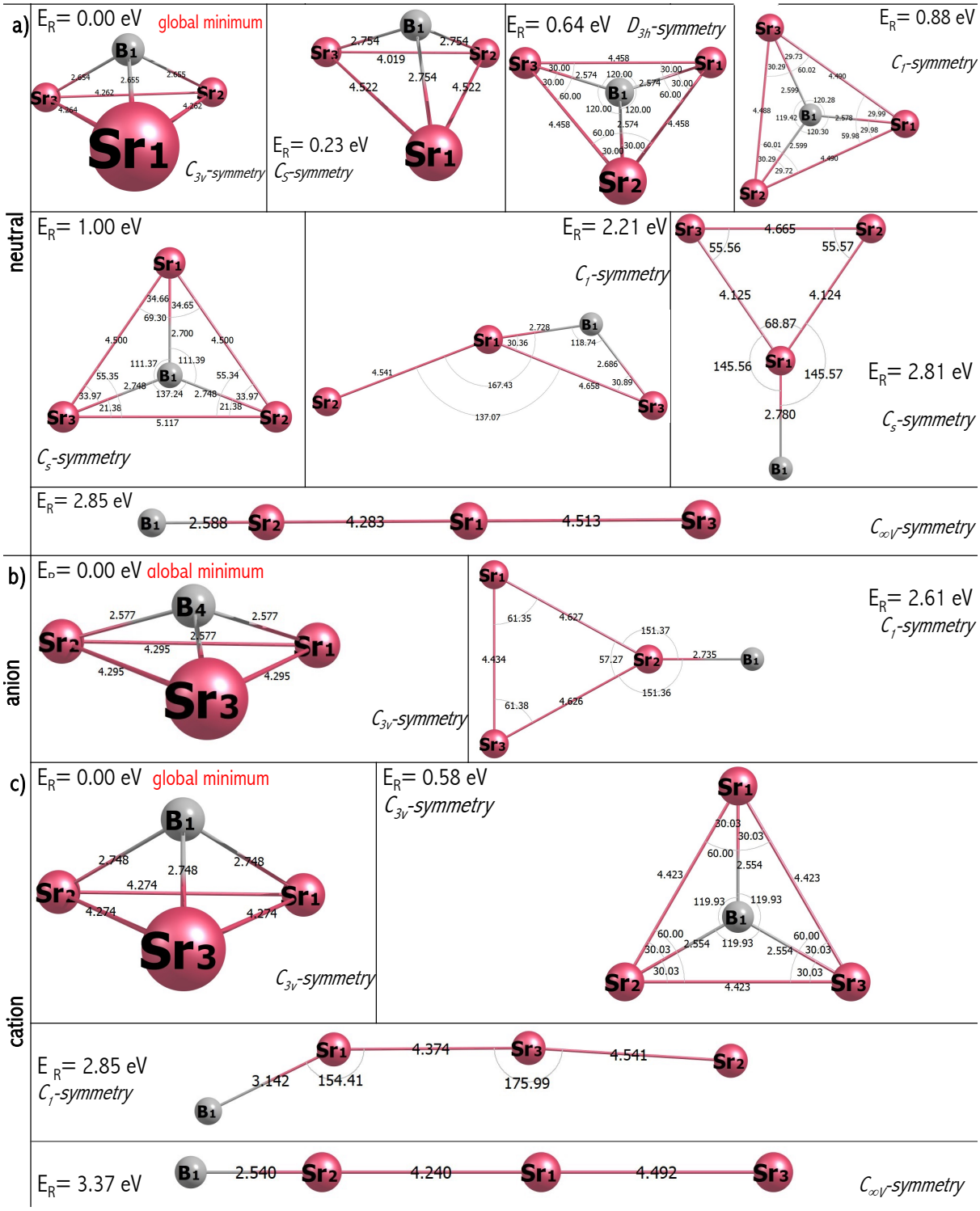

Figure S 2 The MP2/6-311+G(3df)+Def2QZVP equilibrium structures of (a) neutral BSr_3, (b) anionic BSr_3^-, and (c) cationic BSr_3^+ species. Relative energies (E_R in eV) were obtained with respect to neutral, anionic, and cationic global minima (indicated in red), respectively, whose energies were taken as zero. Bond lengths in Å and angles in degrees.

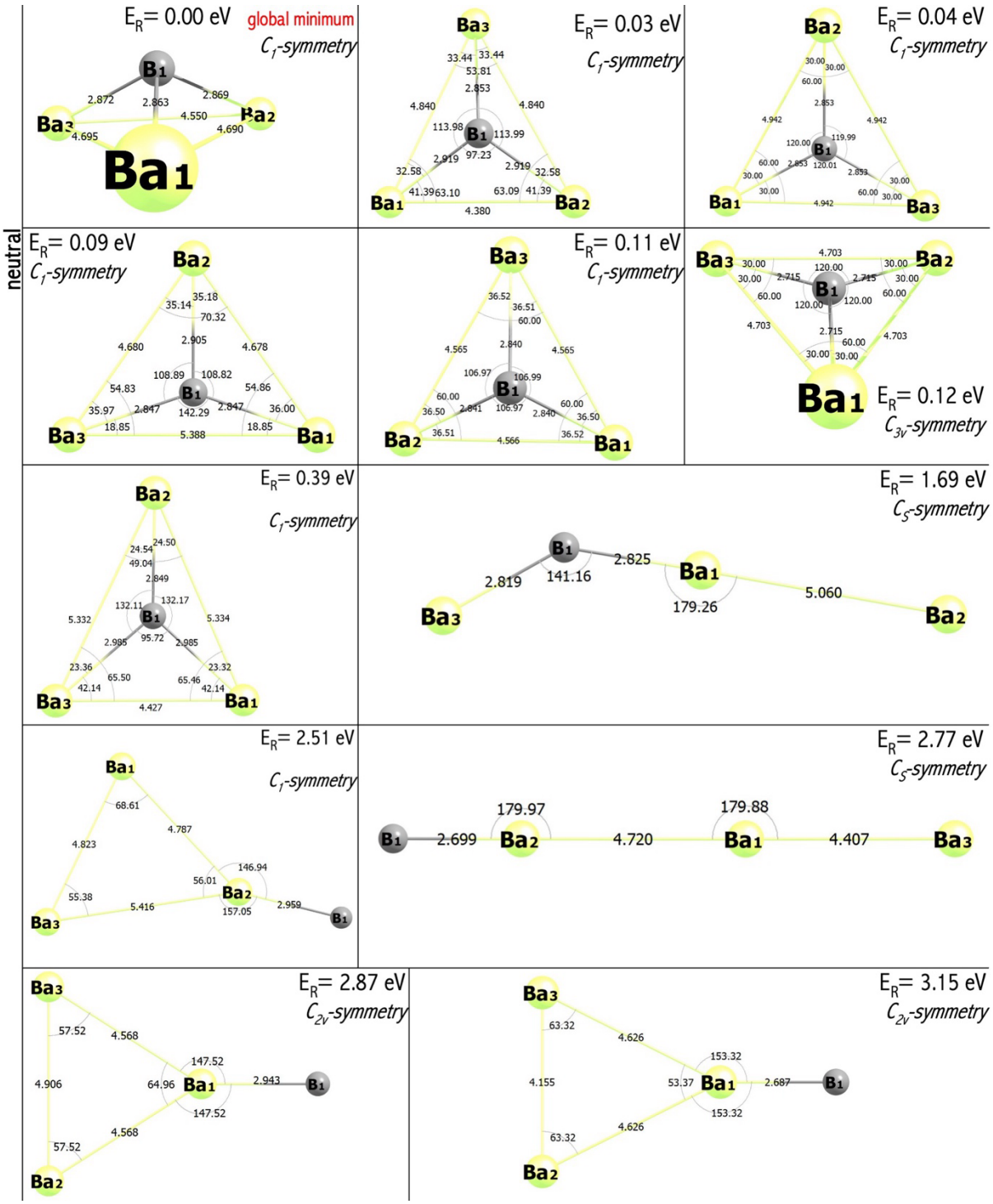

Figure S 3 The MP2/6-311+G(3df)+Def2QZVP equilibrium structures of neutral BBa_3. Relative energies (E_R in eV) were obtained with respect to a global minimum (indicated in red), which energy was taken as zero. Bond lengths in Å and angles in degrees.

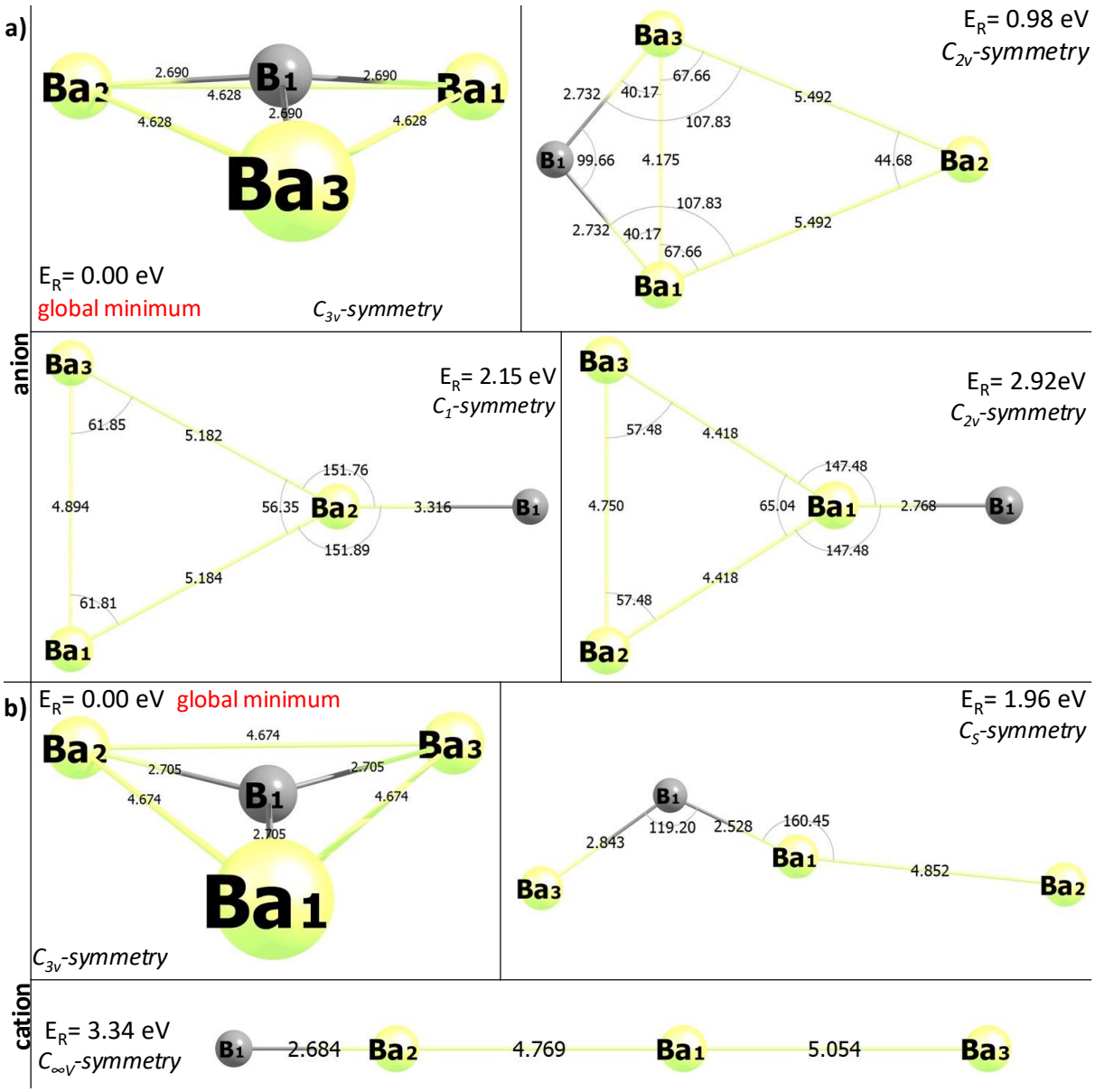

Figure S 4 The MP2/6-311+G(3df)+Def2QZVP equilibrium structures of (a) anionic BBa_3^- and (b) cationic BBa_3^+ species. Relative energies (E_R in eV) were obtained with respect to anionic and cationic global minima (indicated in red), respectively, whose energies were taken as zero. Bond lengths in Å and angles in degrees.

4. Fragmentation channels of BAe_3 (Ae=Be, Mg, Ca, Sr, Ba) ground states

The thermodynamic stability of the BAe_3 (Ae=Be, Mg, Ca, Sr, Ba) systems was examined by calculating the Gibbs free (ΔG_r^{298}) energies of the fragmentation channels of $BAe_3 \rightarrow BAe_2 + Ae$, $BAe_3 \rightarrow BAe + Ae_2$, $BAe_3 \rightarrow BAe + 2Ae$, and $BAe_3 \rightarrow B + 3Ae$ (where Ae is the alkaline earth metal atom). From *Table S 2*, it can be seen that all the dissociation reactions are endothermic. The positive dissociation energies of these fragmentation channels demonstrate that the BAe_3 clusters have thermodynamic stability with respect to the elimination of alkaline earth metal atoms.

Table S 2 *Free enthalpies (ΔH_r^{298} in kcal/mol), entropies [ΔS_r^{298} in cal/(mol K)], and Gibbs free (ΔG_r^{298} in kcal/mol) energies of the fragmentation reactions (at T = 298.15 K, p = 1 atm) obtained at the CCSD(T)/6-311+G(3df)+def2QZVP level of theory for the MP2(full)/6-311+G(3df)+Def2QZVP ground states of BAe_3 (Ae=Be, Mg, Ca, Sr, Ba) clusters.*

Fragmentation path		**ΔH_r^{298}**	**ΔS_r^{298}**	**ΔG_r^{298}**
$BBe_3\rightarrow$	BBe_2 + Be	67.54	29.31	58.80
	B + 3Be	143.68	71.35	122.41
	BBe + 2Be	149.73	52.31	134.13
	BBe + Be_2	148.84	37.51	137.66
$BBe_2Mg\rightarrow$	BBe_2 + Mg	44.38	25.70	36.72
	BBeMg + Be	90.41	28.61	81.89
	BMg + 2Be	98.98	51.66	83.57
	B + 2Be + Mg	120.53	67.74	100.33
	BBe + Be +Mg	126.57	48.70	112.05
$BBeMg_2\rightarrow$	BMg_2 + Be	52.13	26.20	44.32
	BMgBe + Mg	68.57	27.01	60.52
	BMg + Mg + Be	77.13	50.07	62.20
	B + Be + 2Mg	98.68	66.14	78.96
	BBe + 2Mg	104.72	47.10	90.68
$BBe_2Ca\rightarrow$	BBe_2 + Ca	56.48	25.03	49.02
	BBeCa + Be	66.89	29.49	58.09
	B + 2Be + Ca	132.63	67.06	112.63
	BBe + Be + Ca	138.67	48.02	124.35
	BCa + 2Be	167.53	49.91	152.65
	BCa + Be2	166.64	35.11	156.17
$BMg_3\rightarrow$	BMg_2 + Mg	32.12	26.57	24.20
	BMg + 2Mg	57.13	50.44	42.09
	BMg + Mg_2	56.30	38.31	44.87
	B + 3Mg	78.68	66.51	58.85
BBeCaMg$\rightarrow$	BBeCa + Mg	42.46	27.92	34.14
	BMgBe + Ca	78.09	26.36	70.23
	BMg + Ca + Be	86.65	49.42	71.92
	BMgCa + Be	81.37	28.31	72.93
	B + Ca + Be + Mg	108.20	65.49	88.68
	BBe + Mg + Ca	114.24	46.45	100.40
	BCa + Mg + Be	143.10	48.34	128.69
$BCaMg_2\rightarrow$	BMg_2 + Ca	39.48	23.82	32.38
	BMg + Mg + Ca	64.48	47.69	50.27
	BMgCa + Mg	59.21	26.58	51.28
	B + 2Mg + Ca	86.03	63.76	67.02
	BCa + 2Mg	120.93	46.61	107.04
$BBeCa_2\rightarrow$	BCaBe + Ca	50.13	27.32	41.99
	BCa_2 + Be	84.65	25.55	77.04
	B + 2Ca + Be	115.87	64.88	96.52
	BBe + 2Ca	121.91	45.84	108.24
	BCa + Ca + Be	150.77	47.73	136.54
$BCa_2Mg\rightarrow$	BCa_2 + Mg	60.70	23.91	53.57

	$BMg + 2Ca$	70.36	47.17	56.30
	$BCaMg + Ca$	65.09	26.07	57.32
	$B + 2Ca + Mg$	91.91	63.24	73.06
	$BCa + Ca + Mg$	126.81	46.09	113.07
$BCa_3 \rightarrow$	$BCa_2 + Ca$	65.11	25.41	57.54
	$B + 3Ca$	96.33	64.75	77.02
	$BCa + 2Ca$	131.23	47.59	117.04
	$BCa + Ca_2$	129.60	35.25	119.09
$BSr_3 \rightarrow$	$BSr_2 + Sr$	38.03	28.94	29.40
	$BSr + 2Sr$	66.11	49.13	51.47
	$BSr + Sr_2$	64.33	37.45	53.17
	$B + 3Sr$	80.61	64.11	61.50
$BBa_3 \rightarrow$	$BBa_2 + Ba$	39.43	28.71	30.88
	$BBa+ 2Ba$	74.66	48.35	60.24
	$BBa + Ba_2$	72.47	37.08	61.41
	$B + 3Ba$	93.67	63.08	74.86

5. HOMO-LUMO gap and binding energy per atom of neutral and ionic BAe_3 clusters

Table S 3 The eigenvalue of highest occupied molecular orbital (ε_{HOMO}), the eigenvalue of lowest unoccupied molecular orbital (ε_{LUMO}), HOMO-LUMO gap (HL gap), and binding energy per atom (E_b, obtained at the CCSD(T)/6-311+G(3df)+Def2QZVP//MP2(full)/6-311+G(3df)+Def2QZVP level) of $BAe_3^{0/+/-}$ species. All energies in eV.

Species	**Symmetry Group**	**ε_{HOMO} (eV)**	**ε_{LUMO} (eV)**	**HL gap (eV)**	**E_b (eV)**
BBe_3	C_{3v}	-6.568	0.021	6.589	1.44
BBe_3^-	C_{3v}	-1.712	3.345	5.057	2.05
BBe_3^+	C_{3v}	-13.830	-5.369	8.461	2.05
BMg_3	C_{3v}	-5.464	-0.104	5.360	0.73
BMg_3^-	C_{3v}	-1.326	2.646	3.973	1.18
BMg_3^+	C_{3v}	-10.931	-3.896	7.035	1.31
BBe_2Ca	C_s	-5.500	-0.552	4.948	1.32
BBe_2Ca^-	C_s	-1.303	1.937	3.240	1.80
BBe_2Ca^+	C_s	-11.139	-4.232	6.907	1.43
$BCaMg_2$	C_s	-4.973	-0.259	4.715	0.81
$BCaMg_2^-$	C_s	-1.268	1.957	3.225	1.23
$BCaMg_2^+$	C_s	-9.692	-3.663	6.028	1.09
$BBeCa_2$	C_s	-4.817	-0.247	4.570	1.14
$BBeCa_2^-$	C_s	-1.219	1.834	3.052	1.55
$BBeCa_2^+$	C_s	-9.229	-3.453	5.775	1.43
BCa_2Mg	C_s	-4.641	-0.188	4.453	0.88
BCa_2Mg^-	C_s	-1.256	1.845	3.101	1.27
BCa_2Mg^+	C_s	-8.784	-3.247	5.536	1.22
BCa_3	C_{3v}	-4.425	-0.078	4.348	0.93
BCa_3^-	C_{3v}	-1.275	1.817	3.092	1.29
BCa_3^+	C_{3v}	-8.120	-2.944	5.176	1.32
BBe_2Mg	C_s	-6.083	-0.419	5.664	1.19
BBe_2Mg^-	C_s	-1.515	2.686	4.200	1.73
BBe_2Mg^+	C_s	-12.583	-4.781	7.802	1.53
$BBeMg_2$	C_s	-5.733	-0.266	5.467	0.95

$BBeMg_2^-$	C_s	-1.399	2.626	4.025	1.44
$BBeMg_2^+$	C_s	-11.618	-4.278	7.340	1.42
BBeCaMg	C_1	-4.973	-0.259	4.715	1.05
$BBeCaMg^-$	C_1	-1.276	1.934	3.210	1.50
$BBeCaMg^+$	C_1	-10.301	-3.886	6.415	1.26
BSr_3	C_1	-4.119	0.030	4.149	0.87
BSr_3^-	C_{3v}	-1.198	2.610	3.808	1.20
BSr_3^+	C_{3v}	-7.477	-2.718	4.759	1.23
BBa_3	C_1	-3.451	0.053	3.504	1.02
BBa_3^-	C_{3v}	-0.844	2.438	3.282	1.24
BBa_3^+	C_{3v}	-6.634	-2.670	3.964	1.29

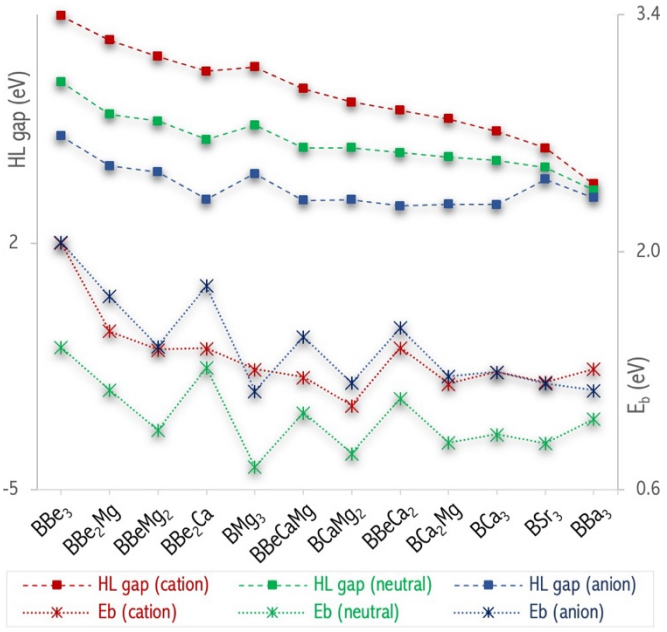

Figure S 5 The HOMO-LUMO gap (HL gap) and binding energy per atom (E_b) of $BAe_3^{0/+/-}$ species. Corresponding estimated data are listed in Table S3.

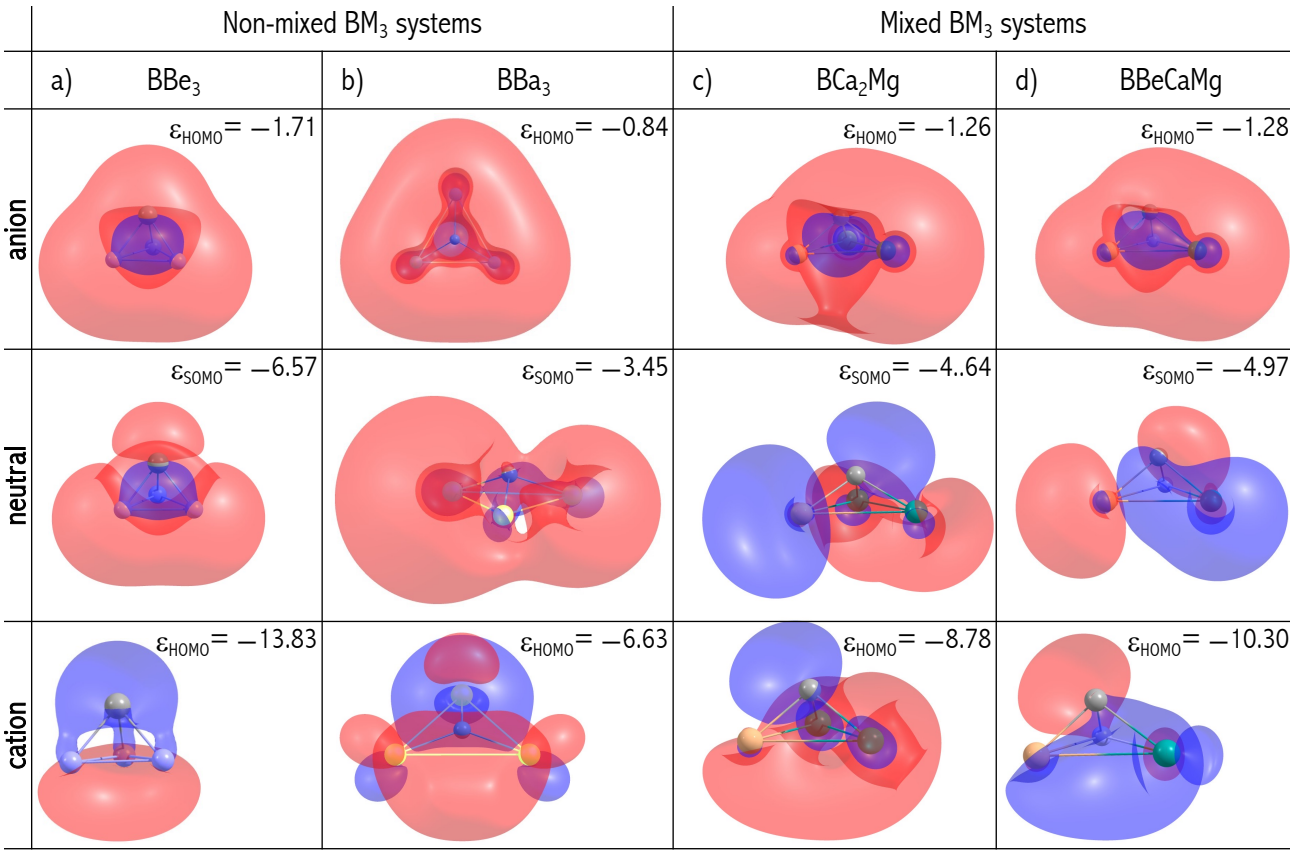

Figure S 6 The highest occupied molecular orbitals (HOMOs) and singly occupied molecular orbitals (SOMOs) of the ground state structures of representative (a-b) non-mixed and (c-d) mixed $BAe_3^{+/-}$ ions and their neutral BAe_3 parents, respectively. The HOMOs and SOMOs are plotted with a fraction of electron density (F_e) equal to 0.8 and their eigenvalues (ε_{HOMO}) are in eV. Contour values used in the plots were obtained with the OpenCubeMan rev.0.01 for the F_e=0.8. [1]

6. Electron localization function (ELF)

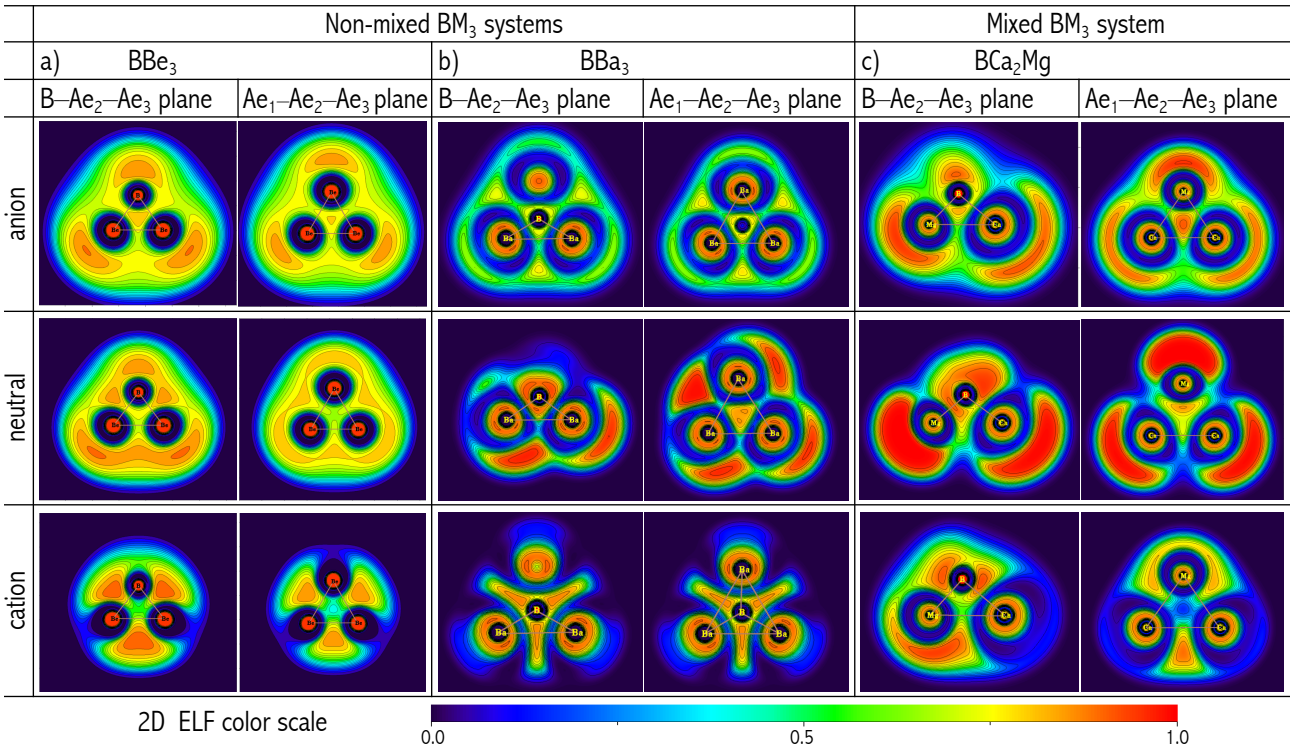

Figure S 7 *Cut-plane electron localization function (ELF) plots of representative (a-b) non-mixed and (c) mixed anionic (top), neutral (middle), and cationic (bottom) BAe_3 clusters in the planes of $B–Ae_1–Ae_2$ and $Ae_1–Ae_2–Ae_3$. The ELF plots were obtained with the Multiwfn v.3.8.* software.[2, 3]

7. Spin densities of neutral clusters

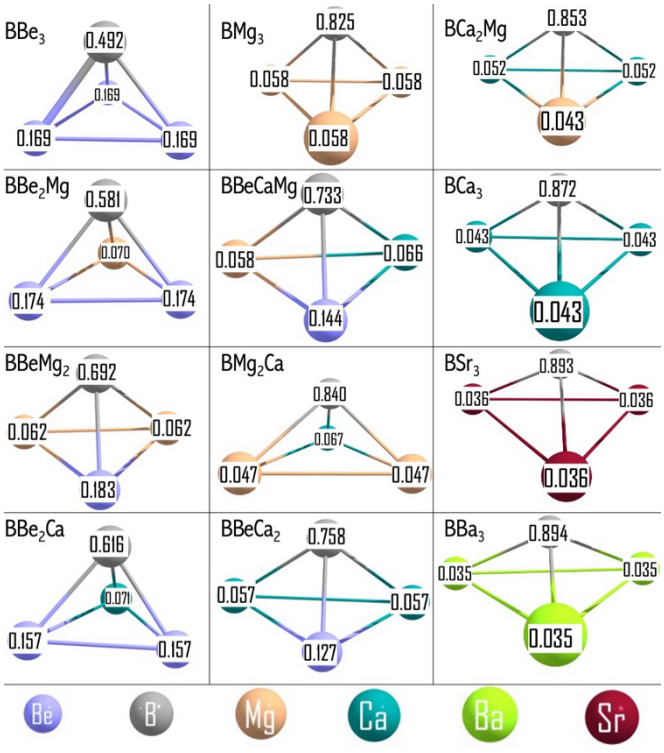

Figure S 8 Natural spin densities of the BAe_3 ground states.

8. Magnetic properties of neutral clusters

We estimated the magnetic susceptibility of neutral cluster using the Perdew–Burke–Ernzerhof (PBE0) hybrid functional. For the PBE0 functional, we incorporated the PBE0-D3 dispersion correction by Grimme *et al.* with Becke–Johnson damping (D3).

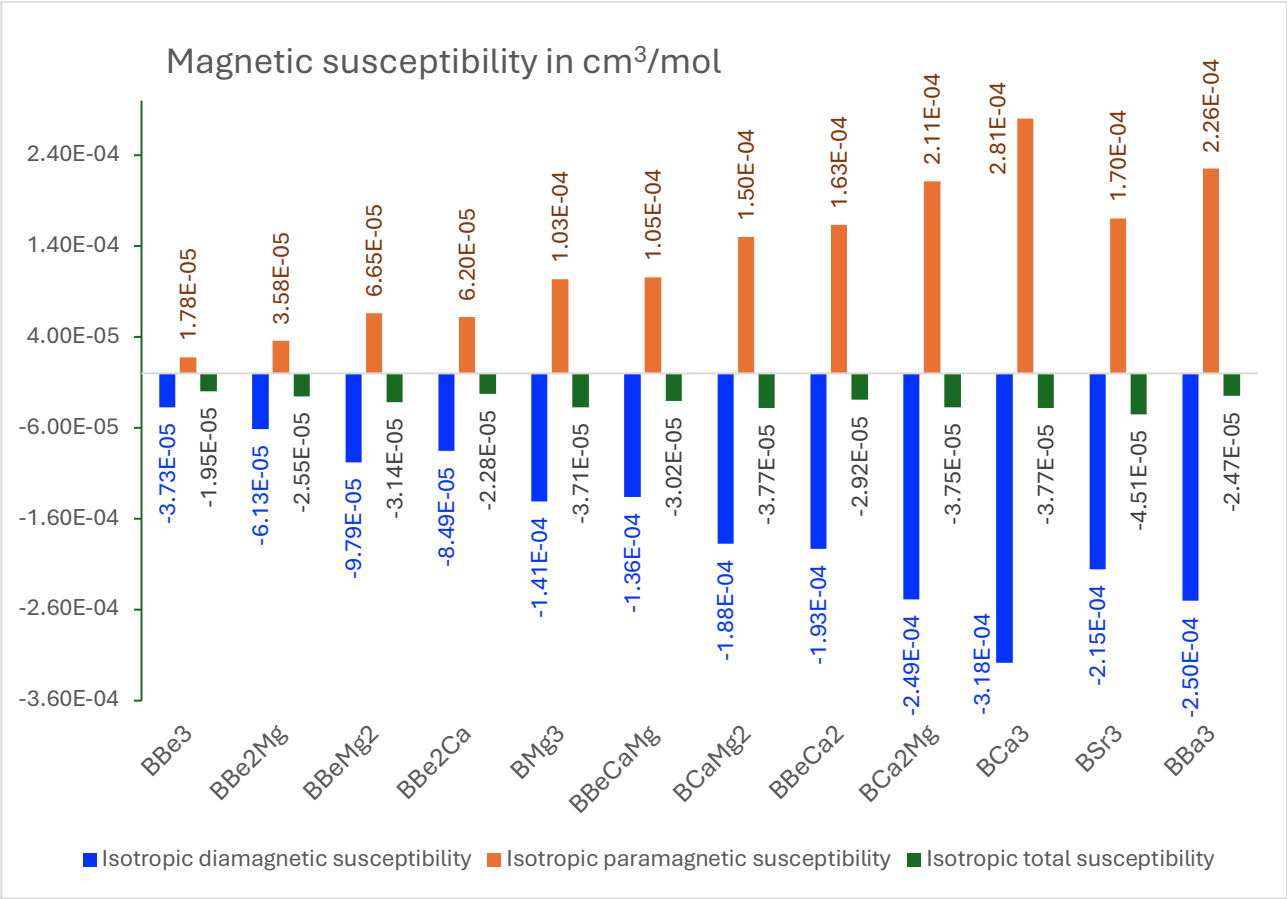

Figure S 9 Isotropic diamagnetic susceptibility, isotropic paramagnetic susceptibility, and net magnetic susceptibility in cm^3/mol. Clusters have been sorted with ascending molecular mass.

9. Mathematical models for ionization energy predictions

We developed mathematical equations for adiabatic ionization energy predictions. The obtained models are exponential or polynomial functions, Table S 8– Table S 9. We examined the goodness of fit via determination coefficient (R^2), R^2_{adj}, summed square of residuals (SSE), root mean squared error (RMSE), and degree of freedom (DFE), whose are defined as follows (Table S 4):

Table S 4 Statistics describing goodness-of-fit and robustness of developed mathematical models, y_i^{obs} referring the observed value of the adiabatic ionization energy for the i^{th} compound, y_i^{pred} is the predicted AIE value for the i^{th} compound, $\bar{y}^{obs}$ is the mean observed value of the AIE, y_i^{pred} is the predicted value for the temporary excluded (cross-validated) i^{th} molecule, n – the number of compounds, and m – the number of fitted coefficients estimated from response AIE values.

Goodness-of-fit parameters	Goodness-of-fit when a new variable is added
Determination coefficient	Adjusted determination coefficient
$\boldsymbol{R^2 = 1 - \frac{\sum_{i=1}^{n}\left(y_i^{obs} - y_i^{pred}\right)^2}{\sum_{i=1}^{n}\left(y_i^{obs} - \bar{y}^{obs}\right)^2}}$	$R^2_{adj} = 1 - \frac{(n-1)\sum_{i=1}^{n}\left(y_i^{obs} - y_i^{pred}\right)^2}{(n-m)\sum_{i=1}^{n}(y_i^{obs} - \bar{y}^{obs})^2}$

Summed square of residuals	Degree of freedom
$\boldsymbol{SSE = \sum_{i=1}^{n} \left(y_i^{obs} - y_i^{pred}\right)^2}$	$DFE = n - m$
Root mean square error of calibration	
$\boldsymbol{RMSE = \sqrt{\frac{\sum_{i=1}^{n} \left(y_i^{obs} - y_i^{pred}\right)^2}{n - m}}}$	

*Table S 5 Mathematical models expressing the relationship between adiabatic ionization energy (AIE, in eV) and decimal logarithm of **molecular mass** for the BAe_3 clusters. Graphical representation of residuals for corresponding mathematical models, 95% confidence bounds, and statistical parameters are also provided. The best model is indicated in green.*

Graphical representation	Model equation and statistical parameters
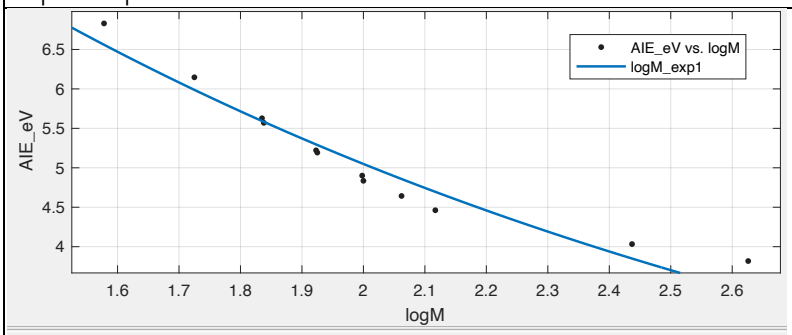	**AIE=a*exp(b*x)**
	Coefficients and 95% confidence bounds
	a 17.4617 13.6245 21.2988
	b -0.6204 -0.7338 -0.5070
	Goodness of fit
	SSE 0.4736
	R^2 0.9417
	DFE 10.0000
	R^2_{adj} 0.9358
	RMSE 0.2176
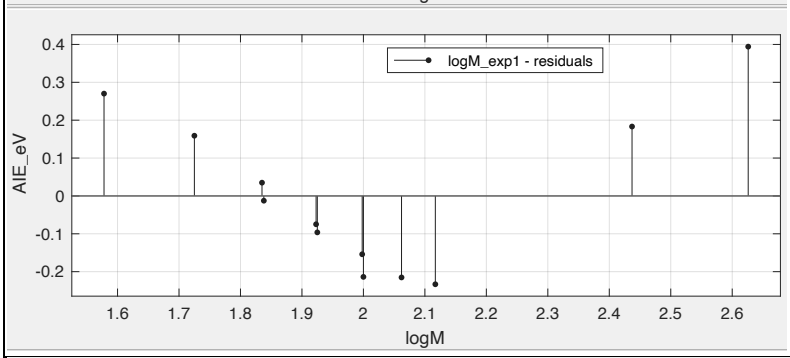	
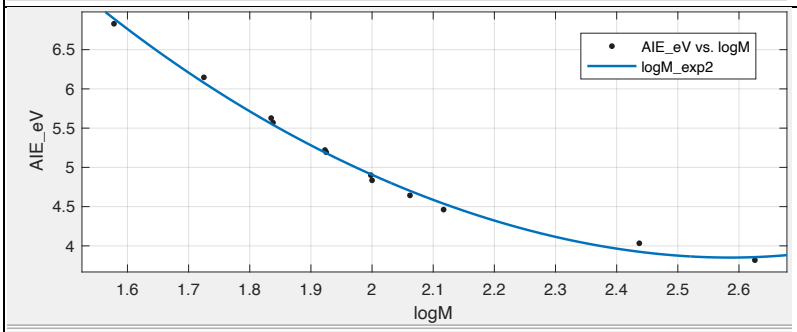	**AIE=a*exp(b*x) + c*exp(d*x)**
	Coefficients and 95% Confidence Bounds
	Value Lower Upper
	a 30.1808 15.4495 44.9120
	b -0.9532 -1.3213 -0.5852
	c 0.0093 -0.0711 0.0897
	d 1.9057 -1.0814 4.8929
	Goodness of fit
	SSE 0.0433
	R^2 0.9947
	DFE 8.0000
	R^2_{adj} 0.9927
	RMSE 0.0736
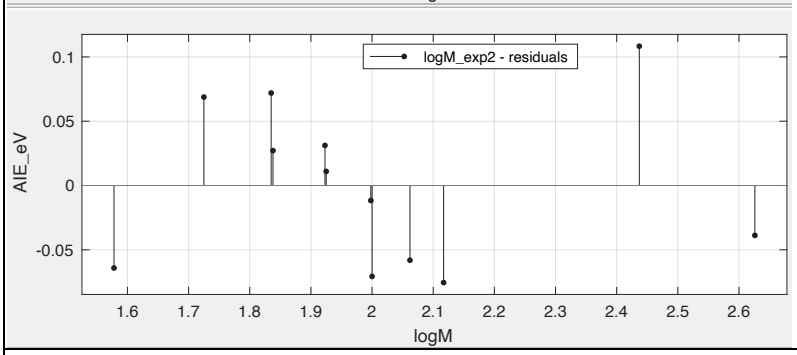	
	AIE=a*x + b
	Coefficients and 95% Confidence Bounds
	Value Lower Upper
	a -2.8111 -3.5748 -2.0474
	b 10.7299 9.1838 12.2759
	Goodness of fit
	SSE 1.0794

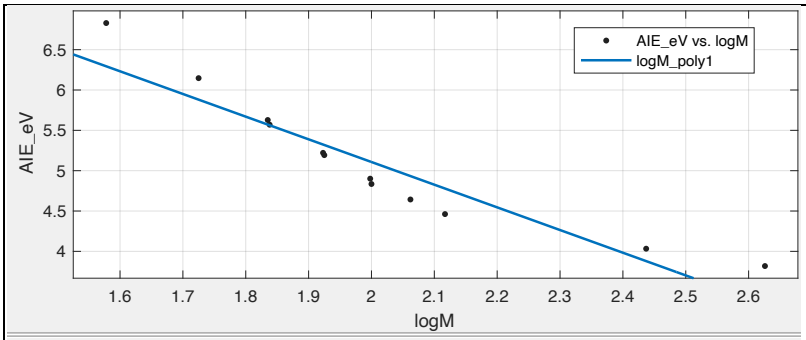

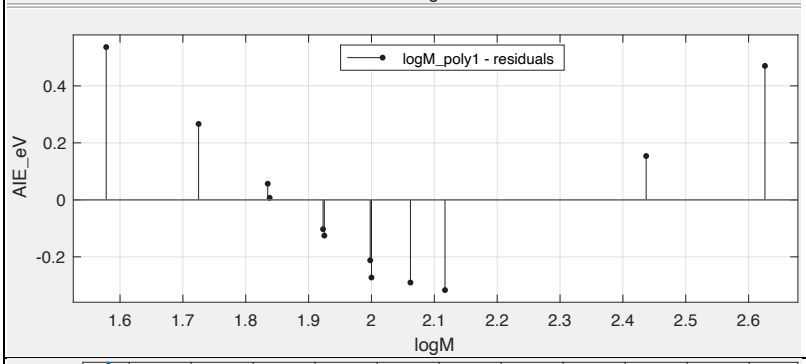

R^2	0.8671
DFE	10.0000
R^2_{adj}	0.8538
RMSE	0.3285

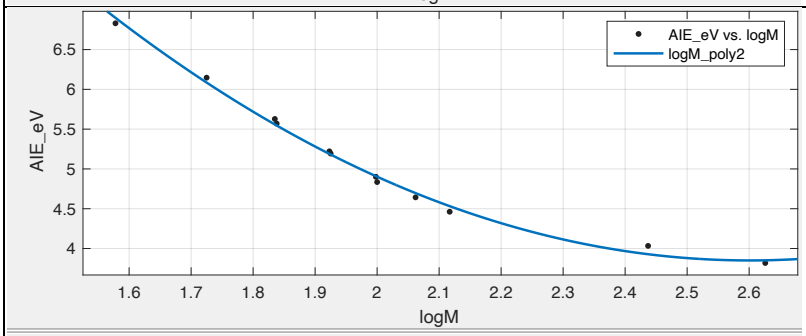

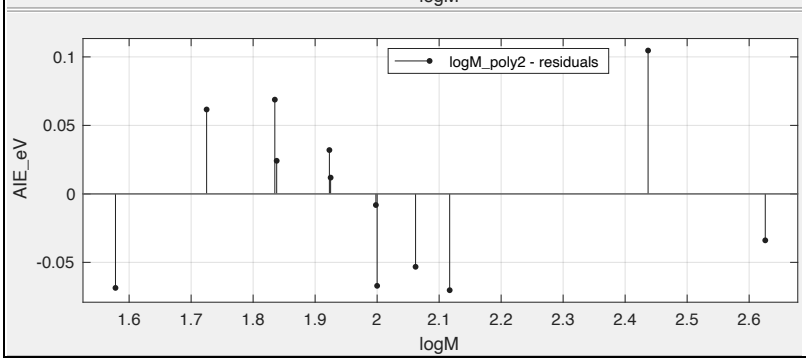

AIE=a*x^2 + b*x + c

Coefficients and 95% confidence bounds

	Value	Lower	Upper
a	2.9136	2.4096	3.4175
b	-15.1558	-17.2993	-13.0124
c	23.5595	21.3132	25.8058

Goodness of fit

SSE	0.0474
R^2	0.9942
DFE	9.0000
R^2_{adj}	0.9929
RMSE	0.0725

*Table S 6 Mathematical models expressing the relationship between adiabatic ionization energy (AIE, in eV) and the sum of **ionization energies** of consisting atoms for the BAe_3 clusters. Graphical representation of residuals for corresponding mathematical models, 95% confidence bounds, and statistical parameters are also provided. The best model is indicated in green.*

Graphical representation	Model equation and statistical parameters

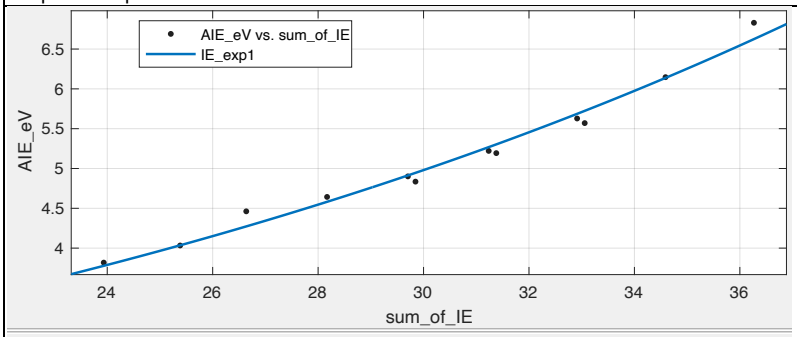

AIE=a*exp(b*x)

Coefficients and 95% confidence bounds

a	1.2701	1.0989	1.4412
b	0.0455	0.0413	0.0498

Goodness of fit

SSE	0.1371
R^2	0.9831
DFE	10.0000
R^2_{adj}	0.9814
RMSE	0.1171

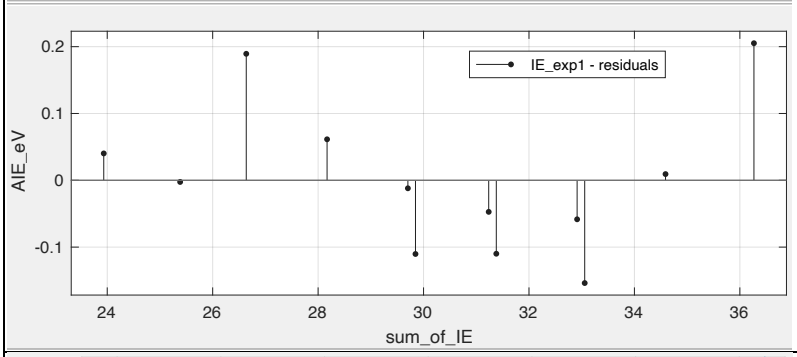

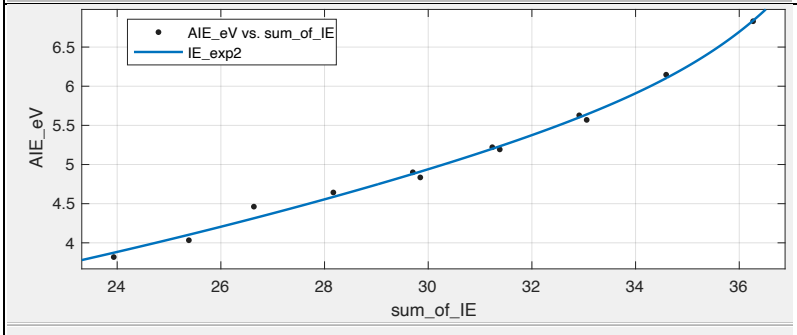

AIE=a*exp(b*x) + c*exp(d*x)

Coefficients and 95% Confidence Bounds

	Value	Lower	Upper
a	1.4982	1.1432	1.8532
b	0.0397	0.0309	0.0484
c	2.1e-10	-7.862e-09	8.282e-09
d	0.5964	-0.4404	1.6331

Goodness of fit

SSE	0.0487
R^2	0.9940
DFE	8.0000
R^2_{adj}	0.9917
RMSE	0.0780

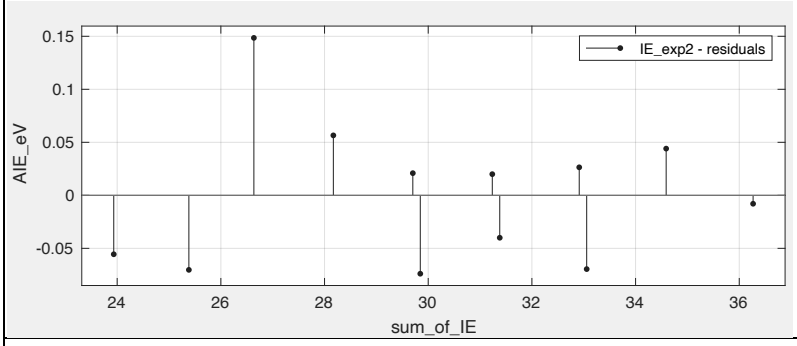

AIE=a*x + b

Coefficients and 95% Confidence Bounds

	Value	Lower	Upper
a	0.1986	0.1754	0.2218
b	-0.9657	-1.6737	-0.2578

Goodness of fit

SSE	0.1671

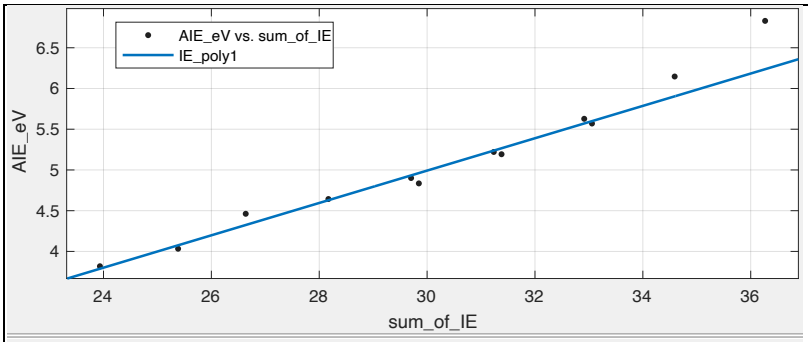

R^2	0.9794
DFE	10.0000
R^2_{adj}	0.9774
RMSE	0.1293

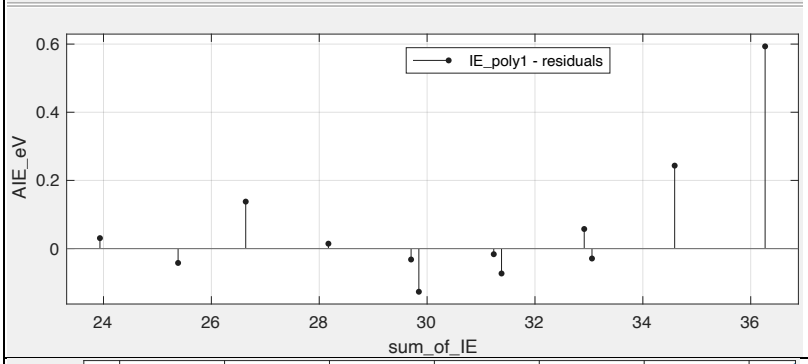

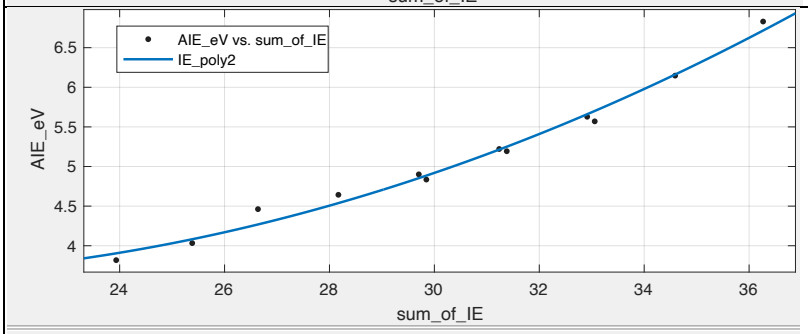

AIE=a*x^2 + b*x + c

Coefficients and 95% confidence bounds

	Value	Lower	Upper
a	0.0097	0.0040	0.0154
b	-0.3546	-0.6973	-0.0119
c	6.8473	1.7525	11.9421

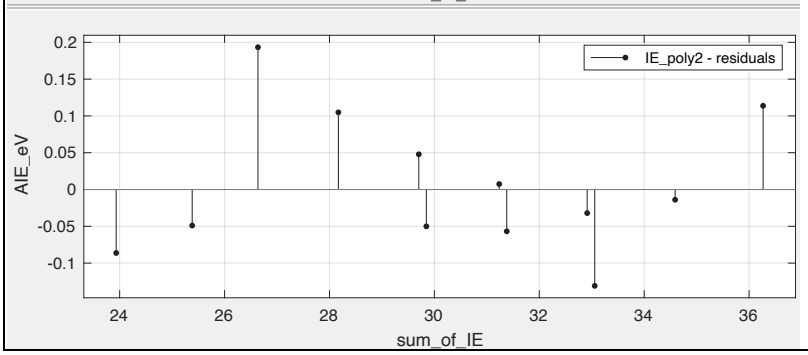

Goodness of fit

SSE	0.1207
R^2	0.9851
DFE	9.0000
R^2_{adj}	0.9818
RMSE	0.1158

*Table S 7 Mathematical models expressing the relationship between adiabatic ionization energy (AIE, in eV) and the **sum of Pauling electronegativity** of consisting atoms for the BAe_3 clusters. Graphical representation of residuals for corresponding mathematical models, 95% confidence bounds, and statistical parameters are also provided. The best model is indicated in green.*

Graphical representation	Model equation and statistical parameters

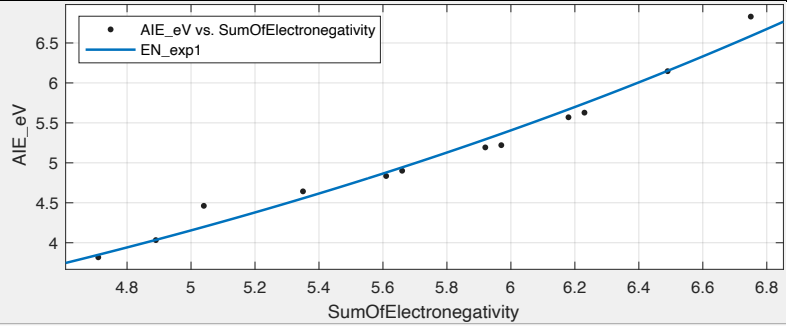

AIE=a*exp(b*x)

Coefficients and 95% confidence bounds

a	1.1133	0.9177	1.3089
b	0.2634	0.2339	0.2929

Goodness of fit

SSE	0.1945
R^2	0.9760
DFE	10.0000
R^2_{adj}	0.9737
RMSE	0.1395

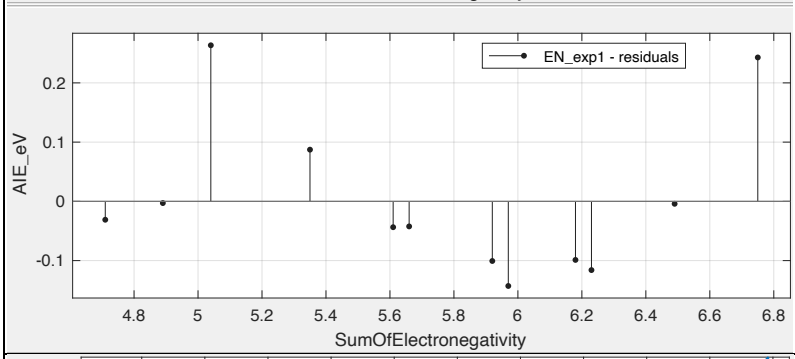

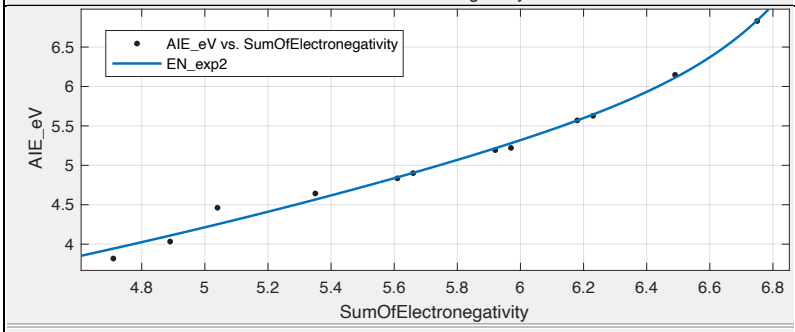

AIE=a*exp(b*x) + c*exp(d*x)

Coefficients and 95% Confidence Bounds

	Value	Lower	Upper
a	1.3460	0.9567	1.7353
b	0.2282	0.1735	0.2829
c	5.255e-13	-2.745e-11	2.85e-11
d	4.1017	-3.6748	11.8783

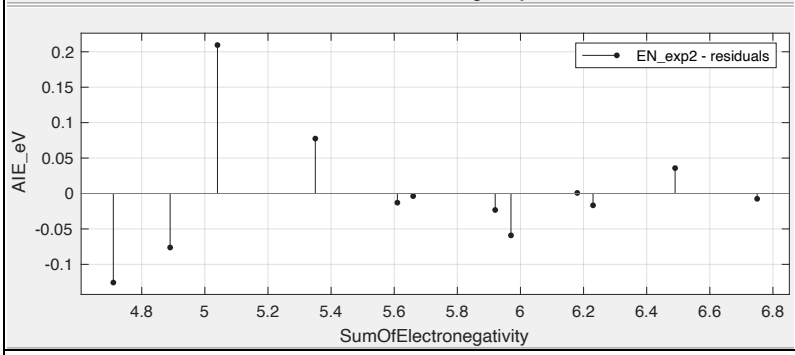

Goodness of fit

SSE	0.0773
R^2	0.9905
DFE	8.0000
R^2_{adj}	0.9869
RMSE	0.0983

AIE=a*x + b

Coefficients and 95% Confidence Bounds

	Value	Lower	Upper
a	1.1918	1.0942	1.2894
b	-1.7955	-2.3584	-1.2327

Goodness of fit

SSE	0.0873

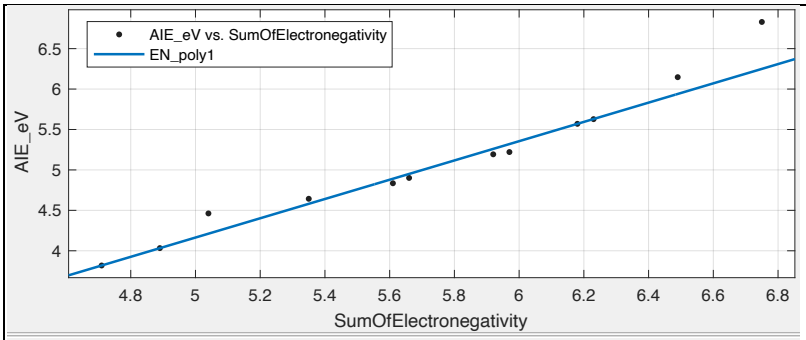

R^2	0.9892
DFE	10.0000
R^2_{adj}	0.9882
RMSE	0.0934

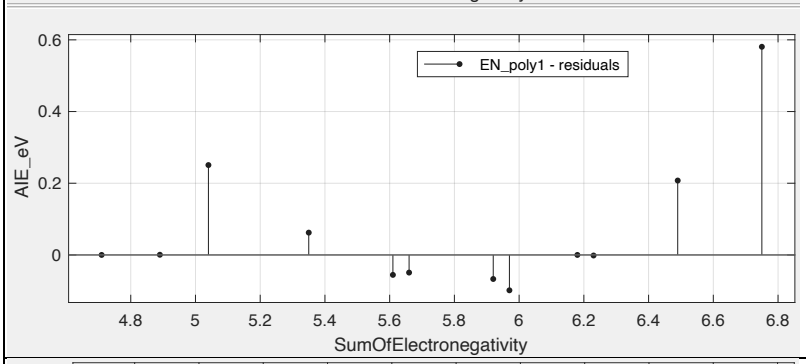

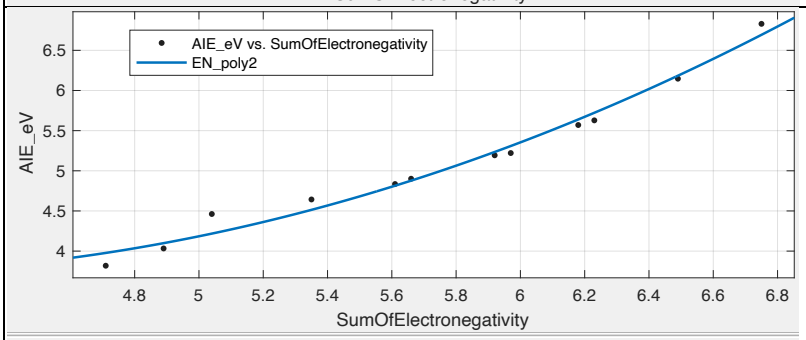

AIE=a*x^2 + b*x + c

Coefficients and 95% confidence bounds

	Value	Lower	Upper
a	0.3522	0.1215	0.5829
b	-2.7045	-5.3359	-0.0731
c	8.9027	1.4655	16.3399

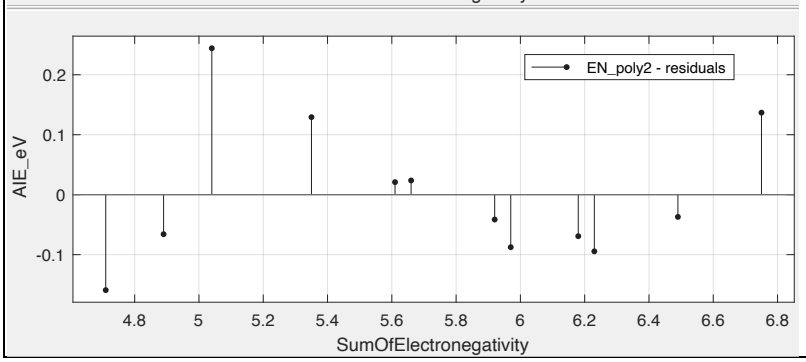

Goodness of fit

SSE	0.1502
R^2	0.9815
DFE	9.0000
R^2_{adj}	0.9774
RMSE	0.1292

*Table S 8 Mathematical models expressing the relationship between adiabatic ionization energy (AIE, in eV) and the **sum of the atomic radius** of consisting atoms for the BAe_3 clusters. Graphical representation of residuals for corresponding mathematical models, 95% confidence bounds, and statistical parameters are also provided. The best model is indicated in green.*

Graphical representation	Model equation and statistical parameters

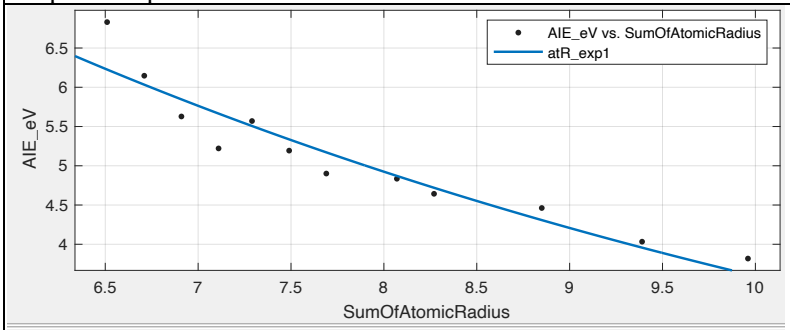

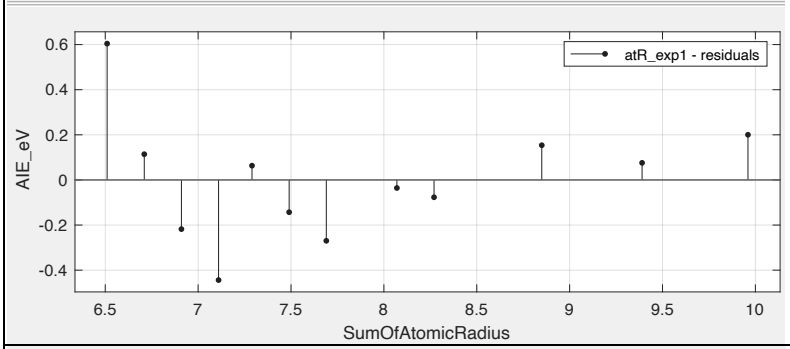

AIE=a*exp(b*x)

Coefficients and 95% confidence bounds

a	17.3403	12.2818	22.3988
b	-0.1573	-0.1957	-0.1190

Goodness of fit

SSE	0.7967
R^2	0.9019
DFE	10.0000
R^2_{adj}	0.8921
RMSE	0.2823

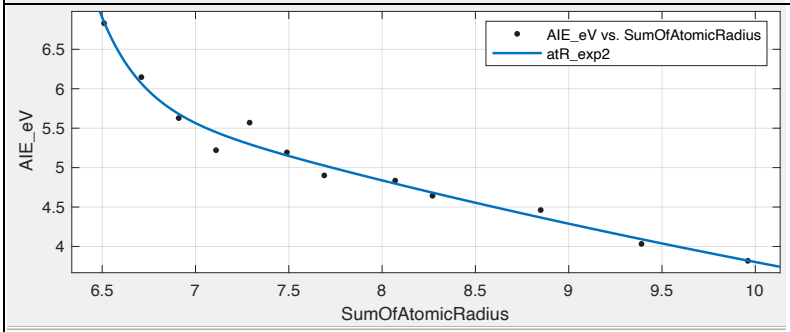

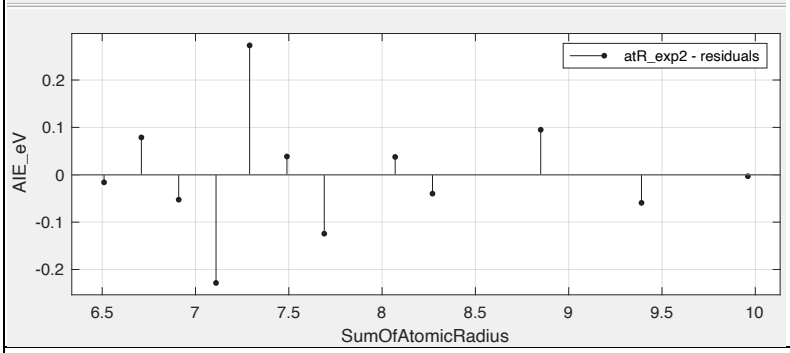

AIE=a*exp(b*x) + c*exp(d*x)

Coefficients and 95% Confidence Bounds

	Value	Lower	Upper
a	1.3688e+13	-4.0840e+14	4.3578e+14
b	-4.6375	-9.3999	0.1250
c	12.6636	9.1880	16.1391
d	-0.1203	-0.1532	-0.0874

Goodness of fit

SSE	0.1685
R^2	0.9792
DFE	8.0000
R^2_{adj}	0.9715
RMSE	0.1451

AIE=a*x + b

Coefficients and 95% Confidence Bounds

	Value	Lower	Upper
a	-0.6455	-0.8118	-0.4793
b	10.1038	8.7866	11.4211

Goodness of fit

SSE	0.7262

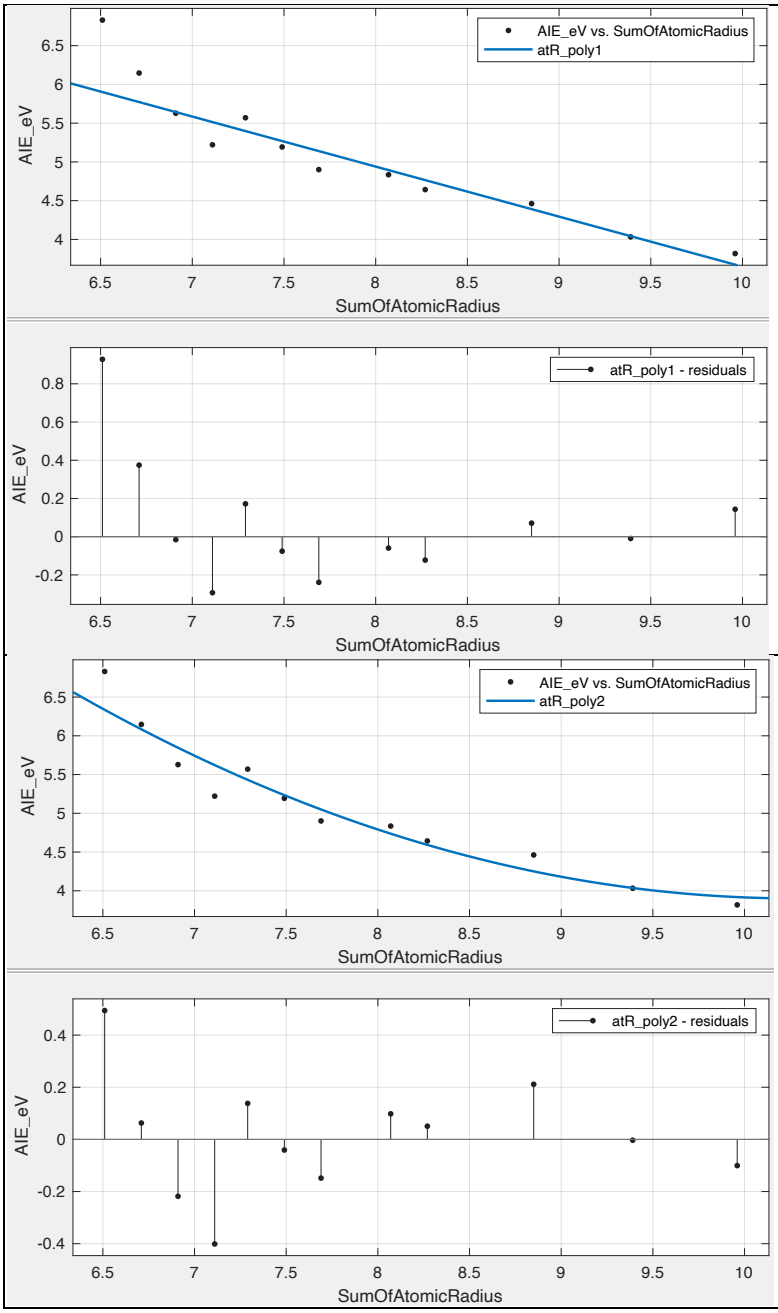

R^2	0.9106
DFE	10.0000
R^2_{adj}	0.9016
RMSE	0.2695

AIE=a*x^2 + b*x + c

Coefficients and 95% confidence bounds

	Value	Lower	Upper
a	0.1716	0.0066	0.3365
b	-3.5265	-6.2317	-0.8212
c	22.0218	11.0928	32.9507

Goodness of fit

SSE	0.6017
R^2	0.9259
DFE	9.0000
R^2_{adj}	0.9094
RMSE	0.2586

To examine the risk of overfitting for the developed polynomial and exponential fits for the descriptors versus modelled endpoint (ionization energy), we analysed (i) difference between predicted and observed ionization energy values by the root squared error (RMSE, Table S 4), (ii) adjusted determination coefficient (R^2_{adj}) across models to assess if added complexity yields genuine benefits, (iii) confidence bounds on model coefficients. Below, we provide general conclusions from analysing of the obtained statistical parameters and visual correlation between the observed AIEs and developed empirical equations.

In general, the visual correlation between the observed AIE values and developed functions shows that exponential (AIE=a*exp(b*x) and linear (AIE=a*x+b) functions are underfitted, see Tables S5-8. Even though the exponential (AIE=a*exp(b*x) and linear (AIE=a*x+b) functions predict well AIE values for the medium-size clusters, they fail for small (such as BBe_3) and large (such as BBa_3) systems.

All two-term exponential fits [AIE=a*exp(b*x) + c*exp(d*x)] reveal coefficients whose confidence intervals cross zero (indicated in red in Tables S5-8), suggesting those terms might not meaningfully contribute to the developed models and could indicate overfitting. Therefore, we consider these two-term exponential equations less reliable and do not recommend using them to predict AIE values.

We estimated the adjusted determination coefficients (R^2_{adj}) of the developed empirical equations to avoid model overfitting. The R^2_{adj} measures how well a regression model explains the variability in the response variable while accounting for the number of fitted coefficients (*m*, see Table S 4) used in the model. Unlike the R^2, which increases with the number of fitted coefficients, the adjusted R^2_{adj} value only increases if adding a coefficient provides enough improvement to overcome the penalty for added complexity - thereby discouraging overfitting. It is beneficial for comparing models with different numbers of predictors and a higher R^2_{adj} suggests a better trade-off between fidelity and simplicity. [4] For the fits utilizing the sum of ionization energies as a descriptor, increasing complexity of the model seems to be justified as the adjusted R^2_{adj} increases from 0.977 (linear function) to 0.982 (quadratic function), see Table S 6. Also, the RMSE value is reduced by 0.014 when the linear equation is replaced with a quadratic function, Table S 6. From both visual correlation and statistical parameters for the empirical equations developed using the sum of ionization energies as a descriptor (x), the $AIE = 6.85 - 0.36x + 0.01x^2$ quadratic fit is the most reliable model for the AIE prediction of BAe_3 clusters.

In the case of the decimal logarithm of molecular mass used as a descriptor, a quadratic fit reveals significantly larger adjusted R^2_{adj} (of 0.993) than a linear function (R^2_{adj}=0.854), see Table S 5. Moreover, the RMSE value of 0.072 obtained for the quadratic function is significantly lower than that obtained for the linear function (RMSE=0.329, Table S 5). The above statistic parameters indicate that the $AIE = 23.56 - 15.16x + 2.91x^2$ quadratic fit, where x represents a decimal logarithm of molecular mass ($log_{10}M$), is a reliable model for the AIE prediction.

Using the sum of the atomic radius as a descriptor of empirical models reveals that employing a quadratic function improves the fit, as the R^2_{adj} and RMSE values read 0.909 and 0.259, respectively. The linear function utilizing the sum of the atomic radius of consisting atoms as a descriptor has the R^2_{adj} equal to 0.902 and RMSE of 0.270, see Table S 8. Thus, employing the $AIE = 22.02 - 3.53x + 0.17x^2$ quadratic instead of a linear function enables obtaining more reliable AIE predictions when x represents the sum of the atomic radius for the BAe_3 clusters.

As soon as the sum of Pauling electronegativity serves as a descriptor of the empirical models for the AIE value prediction, increasing complexity of the model leads to an overfitted quadratic function. In particular, the linear equation reveals R^2_{adj} of 0.988 and RMSE of 0.093, while a quadratic fit reveals the R^2_{adj} of 0.977 and RMSE of 0.129, see Table S 7. The visual correlation between the developed linear function and observed AIE values reveals that the linear equation well predicts AIE values for all BAe_3 clusters but BBe_3 (for which the residual approaches 0.6 eV). Thus, we conclude that the $AIE= -1.795 + 1.192x$ linear equation (where x represents the sum of Pauling electronegativity) can predict AIE values for medium and large BAe_3 clusters and is not recommended for small clusters whose the sum of Pauling electronegativity exceeds 6.75 eV, see Table S 7.

10. Quantitative structure-property relationship (QSPR) modeling

Our mathematical model was validated by internal and external validation. We employed the leave-one-out cross-validation method (LOO) for the internal validation. We assessed the model's robustness by (the cross-validation coefficient) and $RMSE_{CV}$ (the root mean square of cross-validation). [5] The model was further validated with the external test set comprised of data not used to develop the prediction model. Statistics describing the goodness-of-fit and robustness of developed mathematical models were calculated according to formulas presented in Table S 9.

Table S 9 Statistics describing goodness-of-fit and robustness of developed mathematical models, y_i^{obs} referring the observed value of the adiabatic ionization energy for the i^{th} compound, y_i^{pred} is the predicted AIE value for the i^{th} compound, $\bar{y}^{obs}$ is the mean observed value of the AIE, $y_i^{pred_{CV}}$ is the predicted value for the temporary excluded (cross-validated) i^{th} molecule, and n – the number of molecules.

Goodness-of-fit parameters	Robustness of the model	Prediction capability of the model
Determination coefficient	Cross-validation determination coefficient	External validation coefficient
$\boldsymbol{R^2 = 1 - \frac{\sum_{i=1}^{n}\left(y_i^{obs} - y_i^{pred}\right)^2}{\sum_{i=1}^{n}\left(y_i^{obs} - \bar{y}^{obs}\right)^2}}$	$Q_{CV}^2 = 1 - \frac{\sum_{i=1}^{n}\left(y_i^{obs} - y_i^{pred_{CV}}\right)^2}{\sum_{i=1}^{n}(y_i^{obs} - \bar{y}^{obs})^2}$	$Q_{EXT}^2 = 1 - \frac{\sum_{j=1}^{k}\left(y_j^{obs} - y_j^{pred}\right)^2}{\sum_{j=1}^{k}\left(y_j^{obs} - \bar{y}^{obs}\right)^2}$
Root mean square error of calibration	Root mean square error of cross-validation	Root mean square error of prediction
$\boldsymbol{RMSE_C = \sqrt{\frac{\sum_{i=1}^{n}\left(y_i^{obs} - y_i^{pred}\right)^2}{n}}}$	$RMSE_{CV} = \sqrt{\frac{\sum_{i=1}^{n}\left(y_i^{obs} - y_i^{pred_{CV}}\right)^2}{n}}$	$RMSE_{EXT} = \sqrt{\frac{\sum_{j=1}^{k}\left(y_j^{obs} - y_j^{pred}\right)^2}{k}}$

We used the Williams plot to define the applicability domain of the developed QSPR model. In this approach, we verify the presence of compounds within a square created by a leverage threshold (h*=0.86) and an absolute value of standardized cross-validated residual equal to 3. The standardized cross-validated residual values were calculated as a difference between observed and predicted AIEs (**AIE_{obs}**–**AIE_{pred_cv}**). We estimated the leverage values (h_i) as follows:

$$h_i = x_i^T (X^T X)^{-1} x_i \qquad \textit{Eq. S 1}$$

where x_i is the descriptor row-vector of the ith cluster, x_i^T is the transpose of X_i, X is the descriptor matrix, and X^T is the transpose of X matrix.

11. Equilibrium structures of BAe_3/CO_2 (Ae=Be, Mg, Ca, Sr, Ba) species

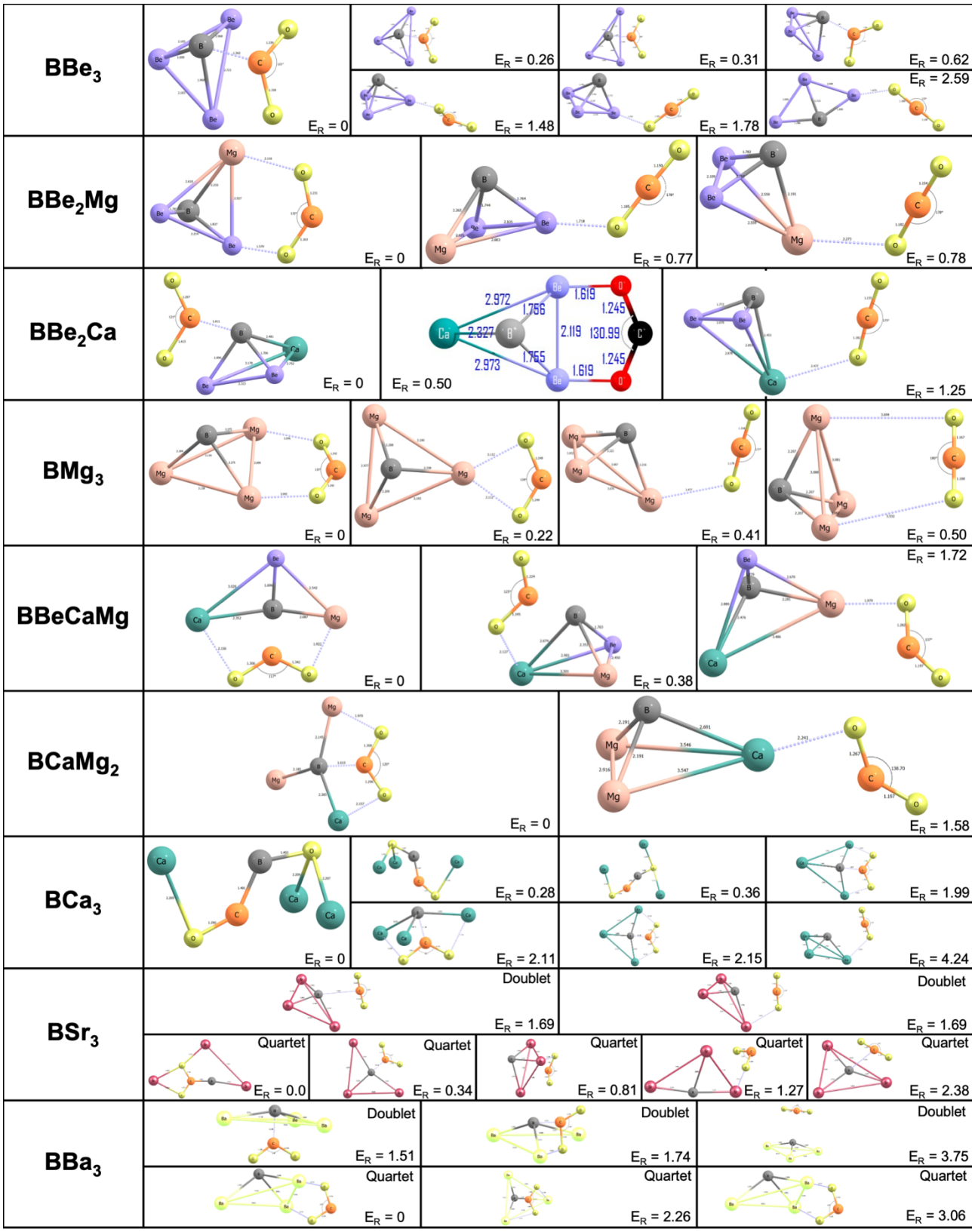

Figure S 10 The MP2/6-311+G(3df)+Def2QZVP equilibrium structures of BAe_3/CO_2 (Ae=Be, Mg, Ca, Sr, Ba) species. Bond lengths in Å. The CCSD(T)/6-311+G(3df)//MP2/6-311+G(3df) relative energies (E_R, in eV) are obtained for BAe_3/CO_2 species with respect to the corresponding global minima. For BSr_3/CO_2 and BBa_3/CO_2 species both doublet and quartet spin states are provided.

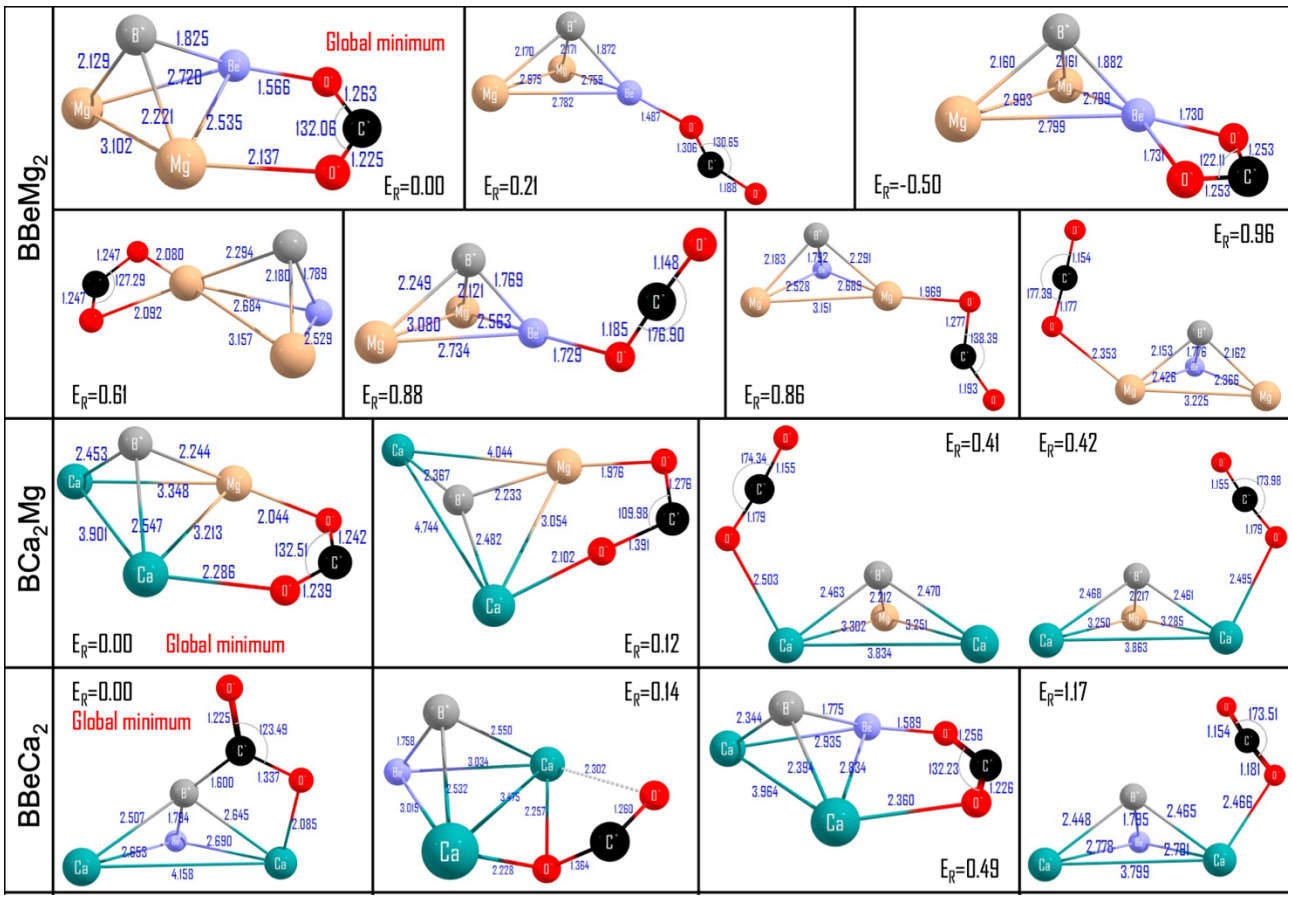

Figure S 11 The MP2(full)/6-311+G(3df) equilibrium structures of $BBeMg_2/CO_2$, BCa_2Mg/CO_2, and $BBeCa_2/CO_2$ species. Bond lengths in Å and the O–C–O valence angle in degrees. *The CCSD(T)/6-311+G(3df)//MP2/6-311+G(3df) relative energies (E_R, in eV) are obtained for BAe_3/CO_2 species with respect to the corresponding global minima (indicated in red).*

12. Optimized structures of BAe_3/N_2 (Ae=Be, Mg, Ca, Sr, Ba) species

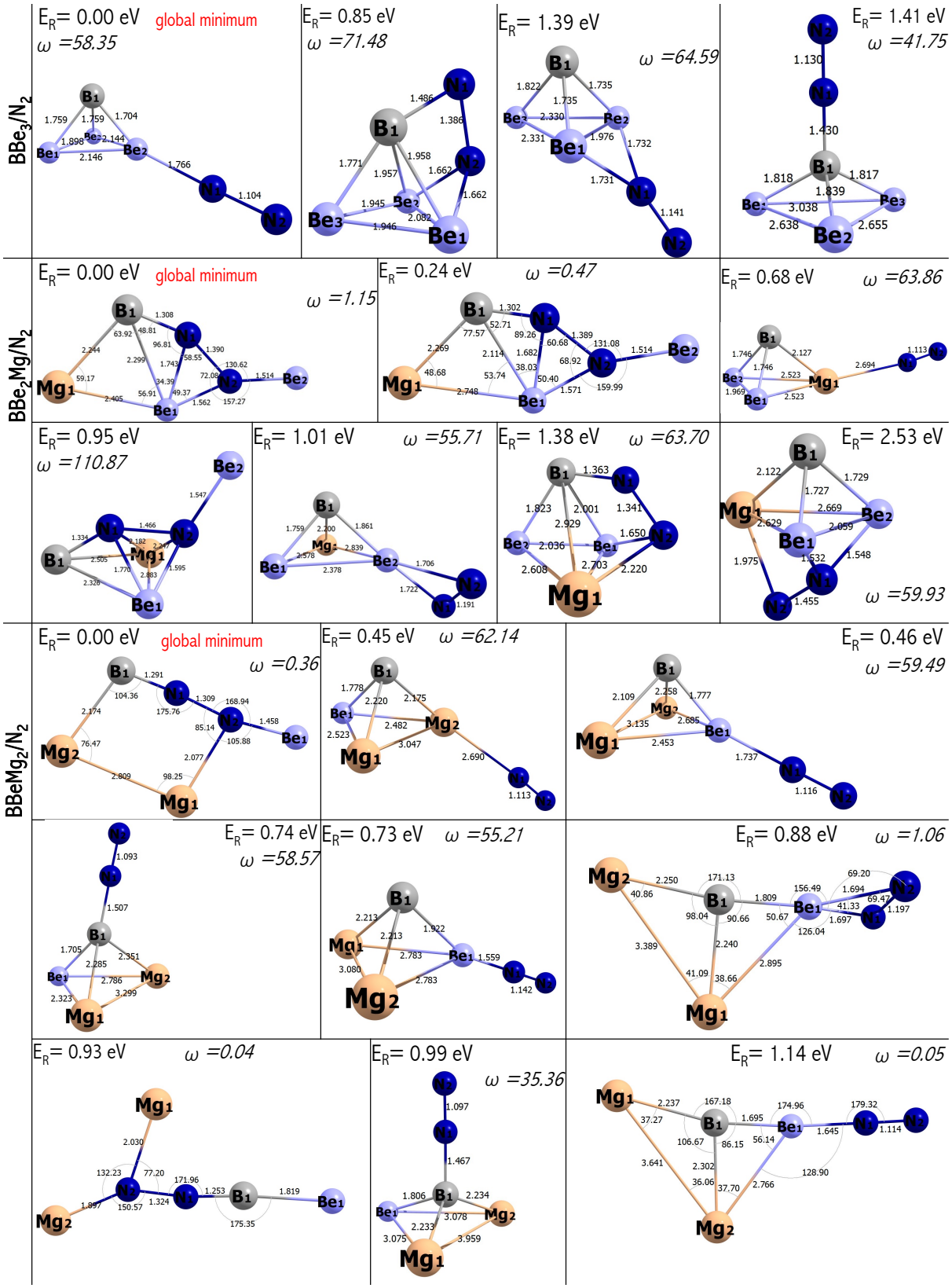

Figure S 12 The MP2/6-311+G(3df) equilibrium structures of BAe_3/N_2 (Ae=Be, Mg) species. Bond lengths in Å. The CCSD(T)/6-311+G(3df)//MP2/6-311+G(3df) relative energies (E_R, in eV) are obtained for BAe_3/N_2 species with respect to the corresponding global minima (indicated in red).

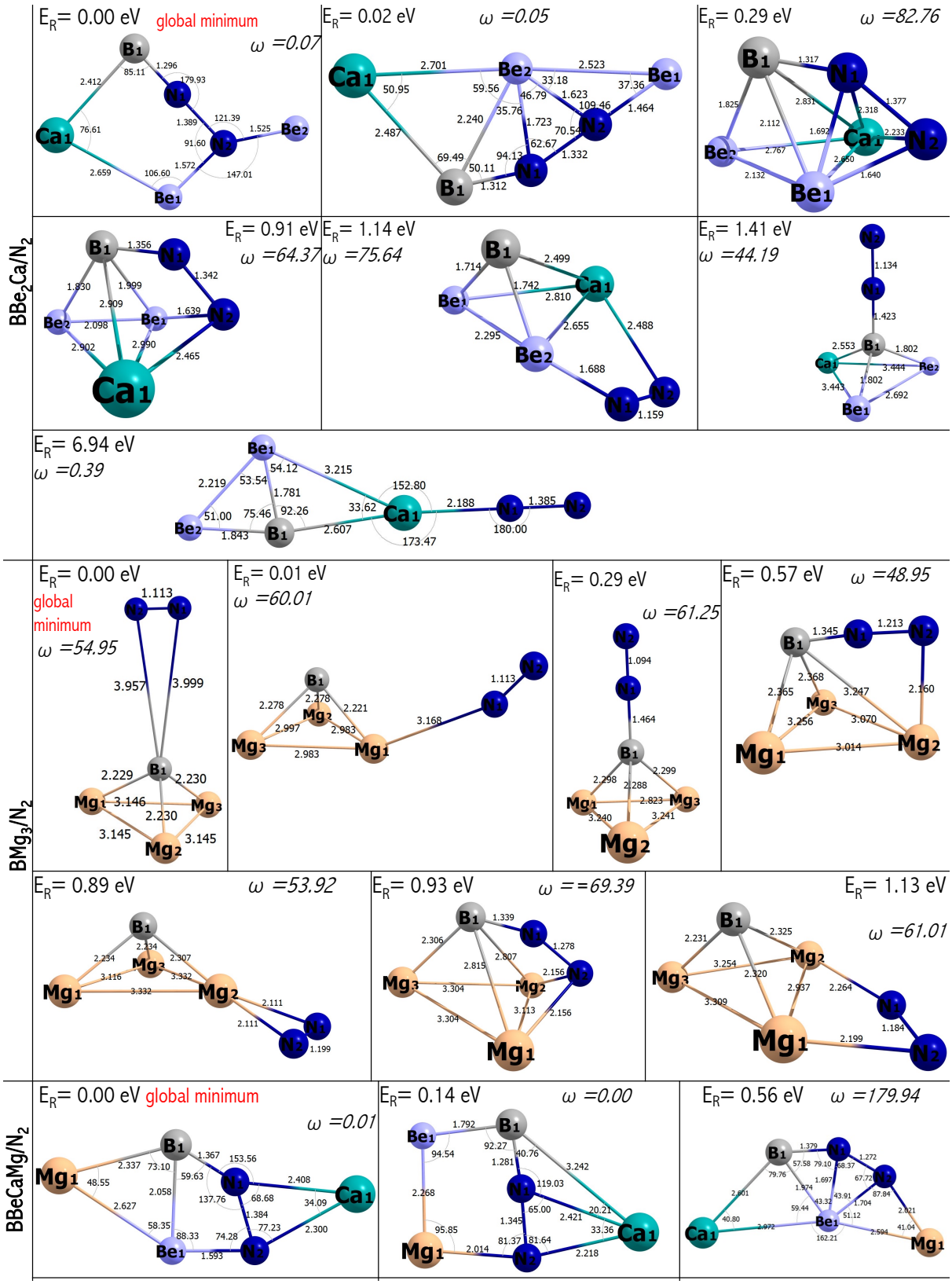

Figure S 13 The MP2/6-311+G(3df) equilibrium structures of BAe_3/N_2 (Ae = Be, Mg, Ca) species. Bond lengths in Å. The CCSD(T)/6-311+G(3df)//MP2/6-311+G(3df) relative energies (E_R, in eV) are obtained for BAe_3/N_2 species with respect to the corresponding global minima (indicated in red).

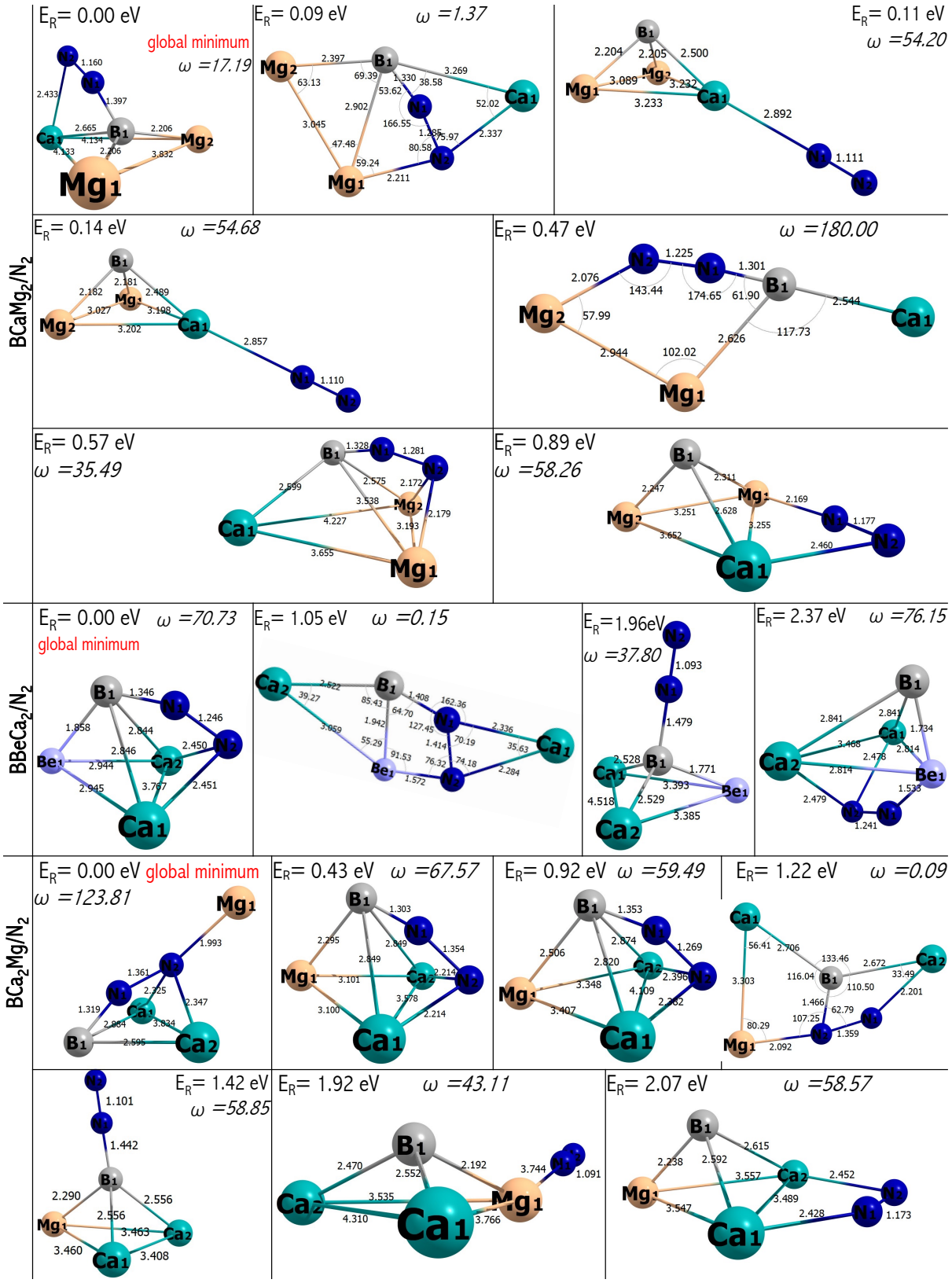

Figure S 14 *The MP2/6-311+G(3df) equilibrium structures of BAe_3/N_2 (Ae=Be, Mg, Ca) species. Bond lengths in Å. The CCSD(T)/6-311+G(3df)//MP2/6-311+G(3df) relative energies (E_R, in eV) are obtained for BAe_3/N_2 species with respect to the corresponding global minima (indicated in red).*

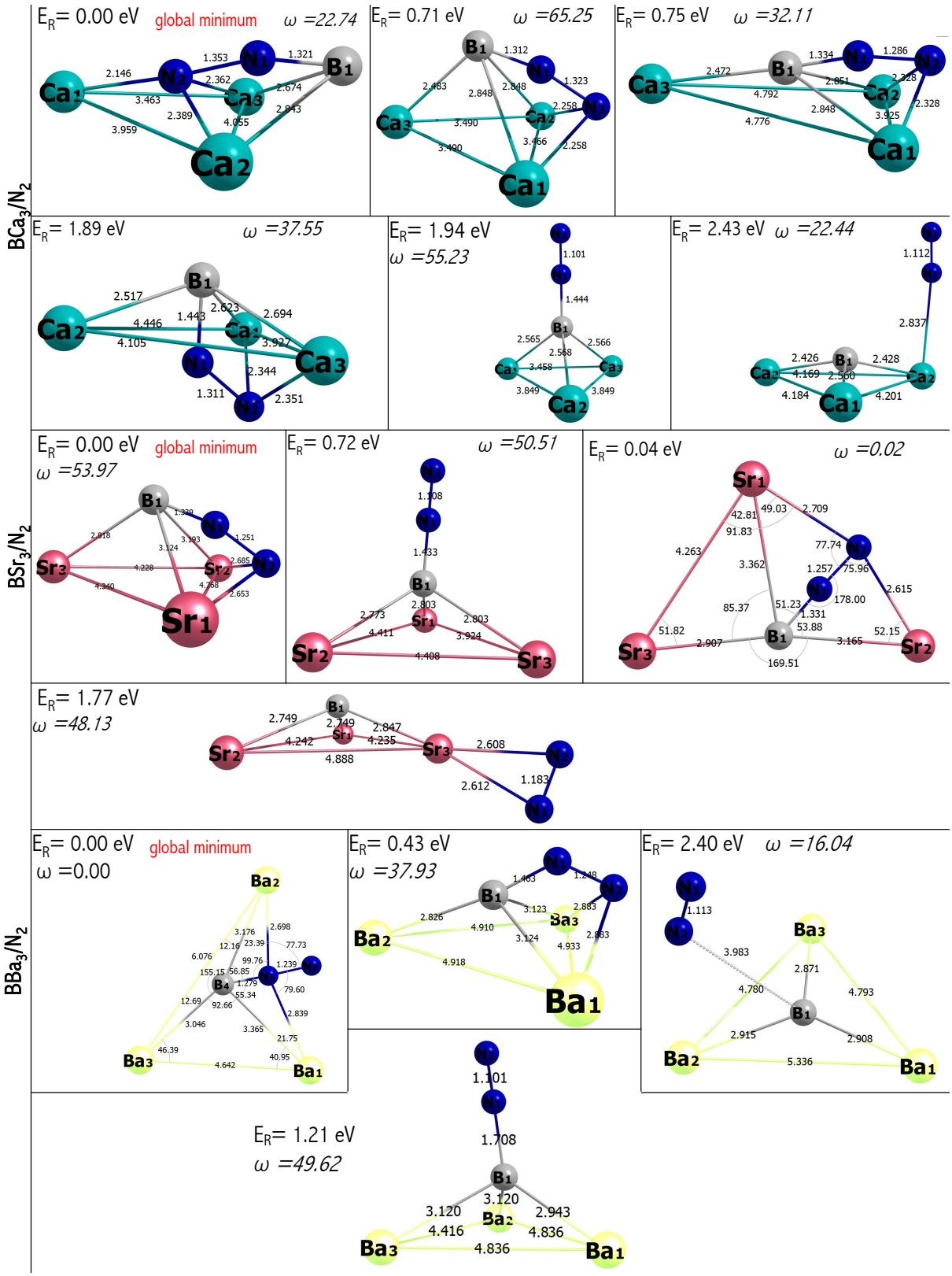

Figure S 15 *The MP2/6-311+G(3df) equilibrium structures of BCa_3/N_2 system and MP2/6-311+G(3df)+Def2QZVP equilibrium structures of BSr_3/N_2 and BBa_3/N_2 systems. Bond lengths in Å. The CCSD(T)/6-311+G(3df)+def2QZVP//MP2/6-311+G(3df)+Def2QZVP relative energies (E_R, in eV) are obtained for BAe_3/N_2 species with respect to the corresponding global minima (indicated in red).*

13. Lifetime of the low-energy BMg_3/N_2 and BSr_3/N_2 local minima

In the case of the BMg_3/N_2 system, we found the comparable energy of the two geometrically stable isomers (not exceeding 0.1 eV, see *Figure S 13* and Figure 12 of the main text). Also, there is no transition

state between these isomeric forms, implying that no barrier must be surmounted to reach the global minimum structure. We assume that upon nearing BMg_3 and N_2 fragments, the BMg_3/N_2 system temporarily stabilizes at a local minimum, characterized by a higher energy (by 0.01 eV) than the global minimum. As the reaction progresses, the system continues to evolve, eventually reaching the global minimum of -0.02 eV lower in energy than the isolated BMg_3 and N_2 fragments, see Figure 12 of the main text.

To further investigate the low-energy isomeric forms of BAe_3/N_2 systems, we estimated the change in Gibbs energy (ΔG) in going from the reactants (N_2 and BAe_3) to the local minimum for the representative BMg_3/N_2 and BSr_3/N_2 systems. In the next step, we obtained rate constants (k) for these transitions following Eq. S 2 :

$$k = \frac{k_B T}{h} e^{-\frac{\Delta G}{RT}} \qquad \textit{Eq. S 2}$$

where k_B is the Boltzmann constant, T is temperature (298.15 K), h is the Planck constant, R is the gas constant, and ΔG is the change in Gibbs free energy in going from the reactants (N_2 and BAe_3) to the local minimum for the BAe_3/N_2 system. The lifetime (τ) of a local minimum was calculated as the inverse of the rate constant:

$$\tau = \frac{1}{k} \qquad \textit{Eq. S 3}$$

The estimated change in Gibbs free energy (ΔG) in going from the reactants (N_2 and BSr_3) to the BSr_3/N_2 local minimum [r(B-N) of 1.965 *Å,* see Figure 13 in the main text] reads 18.39 kcal/mol. The rate constant of this process reads 0.20 s^{-1} , which corresponds to a lifetime of 4.88 s. Due to a sufficiently long lifetime, the BSr_3/N_2 local minimum can serve as a metastable trap for intermediates under standard conditions used in the simulations (gas phase and room temperature).

The change in Gibbs energy (ΔG) in going from the reactants (N_2 and BMg_3) to the BMg_3/N_2 local minimum [Er=0.01 eV, see Figure 12 in the main text] reads 19.90 kcal/mol. The estimated rate of this process reads 0.02 s^{-1} , which corresponds to a lifetime of 62.63 s. The relatively long lifetime of the local minimum and comparable energy of the two geometrically stable BMg_3/N_2 isomers (i.e., not exceeding 0.1 eV) indicate that the interchange between the structures is probably rapid at the temperatures used experimentally.

14. Molecular coordinates

BBe_3 neutral

	Coordinates (Angstroms)		
Atomic number	X	Y	Z
4	0	1.195221	-0.365904
4	-1.035092	-0.597611	-0.365904
4	1.035092	-0.597611	-0.365904
5	0	0	0.878169

BBe_3 anion

	Coordinates (Angstroms)		
Atomic number	X	Y	Z
4	0	1.186015	-0.39078
4	-1.027119	-0.593007	-0.39078
4	1.027119	-0.593007	-0.39078
5	0	0	0.937871

BBe_3 cation

	Coordinates (Angstroms)		
Atomic number	X	Y	Z
4	0	1.262918	-0.373185
4	-1.093719	-0.631459	-0.373185
4	1.093719	-0.631459	-0.373185
5	0	0	0.895644

BCa_3 neutral

	Coordinates (Angstroms)		
Atomic number	X	Y	Z
20	0	2.168178	-0.089884
20	-1.877697	-1.08409	-0.089884
20	1.877697	-1.08409	-0.089884
5	0	0	1.078606

BCa_3 anion

	Coordinates (Angstroms)		
Atomic number	X	Y	Z
20	-0.9324	-1.98909	-0.031146
20	2.189071	0.183527	-0.036587
20	-1.25217	1.798234	-0.158225
5	-0.018006	0.0293	0.90383

BCa_3 cation

	Coordinates (Angstroms)		
Atomic number	X	Y	Z
20	0	2.21508	-0.090627
20	-1.918315	-1.10754	-0.090627
20	1.918315	-1.10754	-0.090627
5	0	0	1.087526

BMg_3 neutral

	Coordinates (Angstroms)		
Atomic number	X	Y	Z
12	0	1.815617	-0.158231
12	-1.57237	-0.907808	-0.158231
12	1.57237	-0.907808	-0.158231
5	0	0	1.13926

BMg_3 anion

	Coordinates (Angstroms)		
Atomic number	X	Y	Z
12	0	1.760495	-0.156424
12	-1.524633	-0.880247	-0.156424
12	1.524633	-0.880247	-0.156424
5	0	0	1.12625

BMg_3 cation

	Coordinates (Angstroms)		
Atomic number	X	Y	Z
12	0	1.815335	-0.164682
12	-1.572127	-0.907668	-0.164682
12	1.572127	-0.907668	-0.164682
5	0	0	1.185713

BSr_3 neutral

	Coordinates (Angstroms)		
Atomic number	X	Y	Z
38	-2.085275	1.307875	-0.041806
38	-0.09084	-2.458669	-0.041772
38	2.176049	1.150678	-0.041834
5	0.000501	0.000879	0.953136

BSr_3 anion

	Coordinates (Angstroms)		
Atomic number	X	Y	Z
38	0	2.479521	-0.029567
38	-2.147328	-1.239761	-0.029567
38	2.147328	-1.239761	-0.029567
5	0	0	0.674123

BSr_3 cation

	Coordinates (Angstroms)		
Atomic number	X	Y	Z
38	0	2.467744	-0.050832
38	-2.137129	-1.233872	-0.050832
38	2.137129	-1.233872	-0.050832
5	0	0	1.158971

BBa_3 neutral

	Coordinates (Angstroms)		
Atomic number	X	Y	Z
5	0.057653	0.000978	-0.985337
56	2.734103	0.037973	0.030598
56	-1.335342	-2.293563	0.028686
56	-1.403909	2.255502	0.028693

BBa_3 anion

	Coordinates (Angstroms)		
Atomic number	X	Y	Z
56	0	2.672214	-0.008922
56	-2.314205	-1.336107	-0.008922
56	2.314205	-1.336107	-0.008922
5	0	0	0.299772

BBa_3 cation

	Coordinates (Angstroms)		
Atomic number	X	Y	Z
56	0	2.698718	-0.005475
56	-2.337158	-1.349359	-0.005475
56	2.337158	-1.349359	-0.005475
5	0	0	0.183977

BBe_2Mg neutral

	Coordinates (Angstroms)		
Atomic number	X	Y	Z
12	-0.253153	1.094471	0
4	-0.253153	-1.259633	0.984961
4	-0.253153	-1.259633	-0.984961
5	1.012612	-0.611317	0

BBe_2Mg anion

	Coordinates (Angstroms)		
Atomic number	X	Y	Z
12	0.268971	1.086777	0
4	0.268971	-1.211084	-1.033128
4	0.268971	-1.211084	1.033128
5	-1.075885	-0.670529	0

BBe_2Mg cation

	Coordinates (Angstroms)		
Atomic number	X	Y	Z
12	-0.258752	1.13799	0
4	-0.258752	-1.293074	1.088245
4	-0.258752	-1.293074	-1.088245
5	1.035007	-0.662257	0

BBe_2Ca neutral

	Coordinates (Angstroms)		
Atomic number	X	Y	Z
4	-0.179605	-1.940885	1.011503
4	-0.179605	-1.940885	-1.011503
20	-0.179605	1.08167	0
5	1.005787	-1.221263	0

BBe_2Ca anion

	Coordinates (Angstroms)		
Atomic number	X	Y	Z
4	-0.204526	-1.657232	1.027445
4	-0.204526	-1.657232	-1.027445
20	-0.204526	0.941322	0
5	1.145345	-1.113717	0

BBe_2Ca cation

	Coordinates (Angstroms)		
Atomic number	X	Y	Z
4	-0.190708	-1.788472	1.065685
4	-0.190708	-1.788472	-1.065685
20	-0.190708	1.00009	0
5	1.067966	-1.138803	0

$BBeMg_2$ neutral

	Coordinates (Angstroms)		
Atomic number	X	Y	Z
4	-1.462979	0.492786	0
12	0.20179	-0.323705	1.565934
12	0.20179	-0.323705	-1.565934
5	0.20179	1.159557	0

$BBeMg_2$ anion

	Coordinates (Angstroms)		
Atomic number	X	Y	Z
4	-1.493099	0.695221	0
12	0.205945	-0.367246	1.532024
12	0.205945	-0.367246	-1.532024
5	0.205945	1.206603	0

$BBeMg_2$ cation

	Coordinates (Angstroms)		
Atomic number	X	Y	Z
4	-1.566852	0.800881	0
12	0.216118	-0.383148	1.577157
12	0.216118	-0.383148	-1.577157
5	0.216118	1.198407	0

$BBeCa_2$ neutral

	Coordinates (Angstroms)		
Atomic number	X	Y	Z
4	-1.575654	0.908727	0
20	0.140058	-0.220552	2.093824
20	0.140058	-0.220552	-2.093824
5	0.140058	1.037432	0

$BBeCa_2$ anion

	Coordinates (Angstroms)		
Atomic number	X	Y	Z
4	-1.570264	0.850494	0
20	0.139579	-0.248779	1.890266
20	0.139579	-0.248779	-1.890266
5	0.139579	1.309834	0

$BBeCa_2$ cation

	Coordinates (Angstroms)		
Atomic number	X	Y	Z
4	-1.614554	0.97149	0
20	0.143516	-0.24863	1.977168
20	0.143516	-0.24863	-1.977168
5	0.143516	1.211848	0

BBeCaMg
neutral

	Coordinates (Angstroms)		
Atomic number	X	Y	Z
4	-0.517499	1.789294	-0.657391
12	-2.033923	-0.551297	-0.078083
20	1.448382	-0.257424	-0.038275
5	-0.498114	0.921373	0.866411

BBeCaMg anion

	Coordinates (Angstroms)		
Atomic number	X	Y	Z
4	-0.654944	1.518199	-0.749275
12	-1.928551	-0.531391	-0.068331
20	1.428867	-0.204566	-0.035026
5	-0.56299	0.879044	0.903518

BBeCaMg cation

Atomic number	X	Y	Z
4	-0.751339	1.640937	-0.673401
12	-1.99821	-0.553483	-0.083359
20	1.497736	-0.198234	-0.043688
5	-0.594167	0.808545	0.913536

BCa2Mg neutral

	Coordinates (Angstroms)		
Atomic number	X	Y	Z
12	-1.700977	1.645893	0
20	0.453594	-0.609666	1.890167
20	0.453594	-0.609666	-1.890167
5	0.453594	0.927183	0

BCa2Mg anion

	Coordinates (Angstroms)		
Atomic number	X	Y	Z
12	-1.6934	1.244946	0
20	0.451573	-0.498063	1.901473
20	0.451573	-0.498063	-1.901473
5	0.451573	0.996634	0

BCa2Mg cation

	Coordinates (Angstroms)		
Atomic number	X	Y	Z
12	-1.741243	1.193336	0
20	0.464332	-0.493381	1.970714
20	0.464332	-0.493381	-1.970714
5	0.464332	1.083041	0

$BCaMg_2$ neutral

	Coordinates (Angstroms)		
Atomic number	X	Y	Z
12	1.019292	0.813541	-1.653037
12	1.019292	0.813541	1.653037
20	-1.477973	-0.797723	0
5	1.019292	-0.714107	0

$BCaMg_2$ anion

	Coordinates (Angstroms)		
Atomic number	X	Y	Z
12	1.019292	0.813541	-1.653037
12	1.019292	0.813541	1.653037
20	-1.477973	-0.797723	0
5	1.019292	-0.714107	0

$BCaMg_2$ cation

	Coordinates (Angstroms)		
Atomic number	X	Y	Z
12	-1.741243	1.193336	0
20	0.464332	-0.493381	1.970714
20	0.464332	-0.493381	-1.970714
5	0.464332	1.083041	0

15. Software Availability

We utilized the Gaussian 16 (Rev. C.01) [6] software for the geometry relaxation and energy computations. We utilized the Multiwfn v.3.6 program [2, 7] for wavefunction analyses. We generated the frontier molecular orbitals with the ChemCraft v.1.8 program, and the contour values used in the plots were estimated with the OpenCubeMan rev.0.01. [1] We used the MATLAB rev.R2024a software [4] for a QSPR modeling.

16. References

1. Haranczyk M, Gutowski M. Visualization of Molecular Orbitals and the Related Electron Densities. *J Chem Theory Comput* (**2008**) *4*: 689-693.
2. Lu T, Chen F. Multiwfn: a multifunctional wavefunction analyzer. *J Comput Chem* (**2012**) *33*: 580-592.
3. Lu T. A comprehensive electron wavefunction analysis toolbox for chemists, Multiwfn. *J Chem Phys* (**2024**) *161*: 082503.
4. MATLAB (R2024a) N, Massachusetts: The MathWorks Inc.; 2024.

5. Sikorska C. Toward predicting vertical detachment energies for superhalogen anions exclusively from 2-D structures. *Chemical Physics Letters* (**2015**) *625*: 157-163.
6. Frisch MJ, Trucks GW, Schlegel HB, Scuseria GE, Robb MA, Cheeseman JR, Scalmani G, Barone V, Petersson GA, Nakatsuji H, Li X, Caricato M, Marenich AV, Bloino J, Janesko BG, Gomperts R, Mennucci B, Hratchian HP, Ortiz JV, Izmaylov AF, Sonnenberg JL, Williams, Ding F, Lipparini F, Egidi F, Goings J, Peng B, Petrone A, Henderson T, Ranasinghe D, Zakrzewski VG, Gao J, Rega N, Zheng G, Liang W, Hada M, Ehara M, Toyota K, Fukuda R, Hasegawa J, Ishida M, Nakajima T, Honda Y, Kitao O, Nakai H, Vreven T, Throssell K, Montgomery Jr. JA, Peralta JE, Ogliaro F, Bearpark MJ, Heyd JJ, Brothers EN, Kudin KN, Staroverov VN, Keith TA, Kobayashi R, Normand J, Raghavachari K, Rendell AP, Burant JC, Iyengar SS, Tomasi J, Cossi M, Millam JM, Klene M, Adamo C, Cammi R, Ochterski JW, Martin RL, Morokuma K, Farkas O, Foresman JB, Fox DJ. Gaussian 16 Rev. C.01. Wallingford, CT2016. p. Gaussian 16 Rev. B.01.
7. Lu T. A comprehensive electron wavefunction analysis toolbox for chemists, Multiwfn. *J Chem Phys* (**2024**) *161*.